Misfolded proteins bind and activate death receptor 5 to trigger apoptosis during unresolved endoplasmic reticulum stress

Authors: Mable Lam[1,2], Scot Marsters[3], Avi Ashkenazi[3,*], and Peter Walter[1,2,*]

Affiliations:

[1] Howard Hughes Medical Institute and Department of Biochemistry and Biophysics, University of California at San Francisco, CA, USA

[2] Department of Biochemistry and Biophysics, University of California at San Francisco, San Francisco, CA 94158, USA.

[3] Cancer Immunology, Genentech, Inc. 1 DNA Way South San Francisco, CA 94080, USA.

* Corresponding author. E-mail: peter@walterlab.ucsf.edu (P.W.); aa@gene.com (A.A.)

Abstract

Disruption of protein folding in the endoplasmic reticulum (ER) activates the unfolded protein response (UPR)—a signaling network that ultimately determines cell fate. Initially, UPR signaling aims at cytoprotection and restoration of ER homeostasis; that failing, it drives apoptotic cell death. ER stress initiates apoptosis through intracellular activation of death receptor 5 (DR5) independent of its canonical extracellular ligand TRAIL; however, the mechanism underlying DR5 activation is unknown. In cultured human cells, we find that misfolded proteins can directly engage with DR5 in the ER-Golgi intermediate compartment, where DR5 assembles pro-apoptotic caspase 8-activating complexes. Moreover, peptides used as a proxy for exposed misfolded protein chains selectively bind to the purified DR5 ectodomain and induce its oligomerization. These findings indicate that misfolded proteins can act as ligands to activate DR5 intracellularly and promote apoptosis. We propose a model in which cells use DR5 as a terminal protein-folding checkpoint before committing to a terminal apoptotic fate.

Introduction

Proper folding of transmembrane and secreted proteins is critical to cell function and intercellular communication. Quality control of protein folding begins in the endoplasmic reticulum (ER) and responds to increased protein-folding demand during physiological or pathophysiological stresses. Accumulation of unfolded or misfolded proteins in the ER, known as ER stress, activates the unfolded protein response (UPR) – a network of intracellular signaling pathways that initially mount a cytoprotective response to restore ER homeostasis but can ultimately switch to a pro-apoptotic program under irresolvable stress (Walter and Ron 2011; Tabas and Ron 2011). Two key UPR sensors, IRE1 and PERK coordinate the decision between cell survival and death through the delayed upregulation of the apoptosis-initiating protein death receptor 5 (DR5) (Lu et al. 2014; Chang et al. 2018).

During ER stress, IRE1 and PERK oligomerize upon directly binding to misfolded proteins, leading to their activation (Karagöz et al. 2017; Wang et al. 2018). PERK activation causes the selective translation of ATF4 and CHOP, which, in addition to upregulating genes that enhance the folding capacity of the ER, promotes the transcription of pro-apoptotic DR5 (Harding et al. 2003; Yamaguchi and Wang 2004). The pro-apoptotic signal is initially counteracted by regulated IRE1-dependent mRNA decay (RIDD) that degrades DR5 mRNA (Lu et al. 2014). Upon prolonged ER stress, PERK exerts negative feedback on IRE1 activity attenuating RIDD, thus de-repressing DR5 synthesis to drive cell commitment to apoptosis (Chang et al. 2018).

DR5 is a pro-apoptotic member of the tumor necrosis factor receptor (TNFR) superfamily that signals from the plasma membrane into the cell in response to extracellular cues (Sheridan et al. 1997; Walczak et al. 1997; A Ashkenazi and Dixit 1998). It is constitutively expressed in various tissue types and forms auto-inhibited dimers in its resting state, analogous to other members of the TNFR family (Spierings et al. 2004; Pan et al. 2019; Vanamee and Faustman 2018). In its canonical mode of activation, binding of the homotrimeric extracellular ligand TRAIL

(also known as Apo2L) (Wiley et al. 1995; Pitti et al. 1996) assembles DR5 into higher-order oligomers (Hymowitz et al. 1999; Mongkolsapaya et al. 1999; Valley et al. 2012). Consequently, DR5 forms intracellular scaffolds in which its cytosolic death domains recruit the adaptor protein FADD and pro-caspase 8 into the "death-inducing signaling complex" (DISC) (Kischkel et al. 2000; Sprick et al. 2000; Jin et al. 2009; Dickens et al. 2012). Upon DISC-mediated dimerization, pro-caspase 8 molecules undergo regulated auto-proteolysis to form active initiator caspase 8 (Muzio et al. 1998). Activated caspase 8 frequently induces the intrinsic mitochondrial apoptotic pathway by truncating Bid, a pro-apoptotic Bcl2 protein, to cause Bax-mediated permeabilization of the mitochondrial outer membrane (Wei et al. 2001; LeBlanc et al. 2002).

While DR5 and caspase 8 are both required for apoptosis during ER stress, we (Lu et al. 2014; Lam et al. 2018), along with other independent groups, found unexpectedly that TRAIL is dispensable for this DR5 activation (Cazanave et al. 2011; Iurlaro et al. 2017; Dufour et al. 2017). Indeed, upon ER stress, most newly synthesized DR5 molecules never make it to the plasma membrane but remain intracellular and thus inaccessible to extracellular ligands (Lu et al. 2014; Iurlaro et al. 2017). Given that at physiological levels DR5 is auto-inhibited until activated by a ligand, it remained a mystery how DR5 is activated in response to ER stress, prompting us to interrogate its intracellular mechanism of activation.

Results

Misfolded proteins induce DR5-dependent apoptosis and can assemble DR5-caspase 8 signaling complexes.

To examine the mechanism of cell death driven by an unmitigated protein folding burden, we induced the exogenous expression of a GFP-tagged form of the glycoprotein myelin protein zero (MPZ) in epithelial cells (Fig 1A). MPZ initially folds in the ER and then travels to the plasma membrane to mediate membrane adhesion in myelin-forming Schwann cells, where

it is normally expressed. Mutations of MPZ that impair folding and cause its intracellular retention activate the UPR, leading to apoptosis in a manner dependent on CHOP (Pennuto et al. 2008). We found that in epithelial cells, titration of even non-mutant, GFP-tagged MPZ to high expression levels resulted in its intracellular accumulation, indicating a compromised MPZ folding state (Fig 1A). Folding-compromised MPZ induced a dose-dependent upregulation of the UPR transcriptional target genes CHOP, BiP, and DR5 (Fig 1–figure supplement 1A). Upregulated DR5 was retained intracellularly (Fig 1A, Fig 1–figure supplement 1B) and occurred concomitantly with cleavage of caspase 8 and its downstream target caspase 3 (Fig 1B). By contrast, low levels of MPZ-GFP expression that exhibited proper plasma membrane localization did not induce caspase 8 or 3 activity (Fig 1A-1B). To determine when caspase 8 became active relative to cytoprotective UPR signaling, we assessed IRE1 activity during high MPZ-GFP expression through analysis of *XBP1* mRNA splicing. As expected, IRE1-mediated *XBP1* mRNA splicing initiated a few hours post-transfection with MPZ-GFP and later attenuated (Fig 1–figure supplement 1C). The upregulation of DR5, caspase activity, and PARP cleavage (another indicator of apoptotic progression) occurred after the attenuation of IRE1 activity, consistent with the hallmarks of terminal pro-apoptotic UPR signaling (Fig 1–figure supplement 1D-1E).

To determine if DR5 was required for apoptosis during this sustained protein misfolding stress, we acutely depleted DR5 mRNA by siRNA prior to overexpressing MPZ-GFP. Knockdown of DR5 significantly reduced PARP cleavage and annexin V staining following overexpression of MPZ-GFP (Fig 1C-1D), which was not observed in control experiments expressing cytosolic GFP. To determine if upregulation of DR5 was sufficient to induce apoptosis, we increased DR5 levels in the absence of ER stress through ectopic expression of CHOP. Comparable levels of CHOP-induced DR5 protein in the absence of ER stress drove drastically lower levels of PARP cleavage and trypan blue staining (demarking apoptotic cells) compared to the presence of misfolded-protein stress (Fig 1–figure supplement 2A, 2C-2D).

These results show that DR5 activation does not occur spontaneously after its upregulation but requires additional input signals conveyed by ER stress.

To assess the molecular composition of activated DR5 assemblies formed in response to ER stress, we measured caspase 8 activity in cell extracts fractionated through size exclusion chromatography. We detected increased caspase 8 activity in high-molecular weight (MW) fractions of cells transfected with MPZ-GFP relative to GFP (Fig 1E). The fractions contained DR5 complexes and co-eluted with full-length MPZ-GFP but not GFP-degradation products (Fig. 1E, lanes 2 and 4). Pull-down of DR5 from cell lysates enriched for FADD and MPZ-GFP (Fig 1–figure supplement 3A), suggesting that the co-elution of DR5 and MPZ-GFP in the high MW fractions resulted from their physical association. To test if MPZ physically interacted with activated DR5 complexes, we immunoprecipitated MPZ-GFP and detected DR5, FADD, and caspase 8 (both full-length p55 and its cleaved form p43) (Fig 1F, Fig 1–figure supplement 3B). Furthermore, MPZ-GFP immunoprecipitates contained 2-3-fold more caspase 8 activity compared to empty beads (Fig 1G, Fig 1–figure supplement 3C), indicating that they contained assembled DISC in a similar degree as seen after affinity purification of TRAIL-ligated DR5 (Hughes et al. 2013). In contrast, pull-down of cytosolic GFP did not enrich for DR5, FADD, or caspase activity (Fig 1F-1G), confirming the selectivity for ER-folded MPZ-GFP.

To determine if misfolded proteins generally induced caspase activity through association with DR5, we overexpressed GFP-tagged forms of two other ER-trafficked proteins, rhodopsin (RHO) and proinsulin (INS), which are also associated with CHOP-dependent cell death pathologies (W.-C. Chiang et al. 2016; Oyadomari et al. 2002). Sustained overexpression of both RHO-GFP and INS-GFP upregulated BiP and CHOP mRNAs (Fig 1–figure supplement 4A) and induced *XBP1* mRNA splicing (Fig 1–figure supplement 4B). Both proteins formed SDS-insoluble aggregates and induced PARP cleavage and annexin V staining in a DR5-dependent manner (Fig 1–figure supplement 4C-4E). By contrast, immunoprecipitation of RHO-GFP enriched for DR5 protein and caspase 8 activity more robustly than INS-GFP (Fig 1–figure

supplement 5), despite inducing DR5-dependent apoptosis to a similar extent. This indicates that misfolded proteins differ in their propensity to directly engage the DR5-assembled DISC, and that other misfolded substrates—caused by the ectopically overexpressed ER-trafficked protein—may mediate direct DR5 activation. Thus, as exemplified by MPZ and RHO, a selective subset of misfolded proteins in the secretory pathway can engage DR5 to form oligomeric complexes that induce caspase 8 activation.

Misfolded protein engages DR5 at the ER-Golgi intermediate compartment, inducing active DR5 signaling clusters.

To explore where within in the cell DR5 associated with misfolded protein, we used confocal imaging of fixed cells for immunofluorescence. These analyses revealed that intracellular MPZ-GFP and DR5 appeared in discrete puncta that often overlapped (Fig 2A). DR5 siRNA knockdown eliminated the DR5 signal, confirming the specificity of the DR5 antibody (Fig 2–figure supplement 1A, right panel). Similarly, overexpression of RHO also resulted in intracellular puncta that frequently co-localized with DR5 clusters (Fig 2–figure supplement 1B). Quantification of the mean Pearson's correlation per cell demonstrated statistically significant overlap with DR5 signal for both GFP-tagged MPZ and RHO (Fig 2–figure supplement 1C), indicating that these misfolded proteins accumulate in the same compartment as DR5.

Previous findings suggested that DR5 is retained near the Golgi apparatus during ER stress (Lu et al. 2014). We confirmed co-localization with the purported Golgi marker RCAS1, as previously reported (Fig 2– figure supplement 1D). However, we observed little overlap in DR5 staining with another *cis*-Golgi marker, giantin (Fig 2E). To resolve this discrepancy, we employed subcellular fractionation as an orthogonal biochemical approach. Separating organelle membranes revealed that RCAS1, DR5, and MPZ-GFP co-sedimented in fractions containing ERGIC53, a marker of the ER-Golgi intermediate compartment (ERGIC), but not with

157 those containing giantin (Fig 2B). Notably, a portion of FADD, a cytosolic protein expected to
158 exclusively remain in the topmost, cytosolic fraction, migrated into the second fraction of the
159 gradient, indicating its association with the ERGIC membranes. Consistent with the presence of
160 FADD, the first and second ERGIC-associated fractions harbored the majority of the caspase 8
161 activity in the cell lysate (Fig 2C), indicating the presence of active DR5 DISCs. Moreover,
162 immunofluorescence with quantification of the mean correlation per cell demonstrated the co-
163 localization of DR5 with the ERGIC rather than with the Golgi (Fig 2D, 2F).
164 To determine when DR5 accumulates at the ERGIC relative to misfolded proteins, we
165 compared the immunofluorescence of cells fixed at 20 hours (before the onset of caspase
166 activity) and at 24 hours post-transfection (after the onset of caspase activity, Fig 1–figure
167 supplement 1E). Intracellular puncta of MPZ appeared at 20 hours, preceding the appearance
168 of DR5 clusters at 24 hours (Fig 2–figure supplement 2A). Between 20 and 24 hours, the
169 correlation of DR5 and ERGIC53 increased, whereas the correlation of MPZ with ERGIC53
170 remained steady, indicating that DR5 accumulated after saturation of MPZ levels at the ERGIC
171 (Fig 2–figure supplement 2B-2C). By contrast, the mean Pearson's correlation with giantin
172 approached zero for both MPZ and DR5 at 24 hours post-transfection (Fig 2–figure supplement
173 2B, Fig 2F). These results confirm the localization of DR5 and misfolded protein at the ERGIC
174 under conditions of unmitigated ER stress.
175
176 *Polypeptide sequences of mammalian ER-trafficked protein directly bind to the DR5 ectodomain*
177 *and induce its oligomerization..*
178 With evidence of a physical association between misfolded protein and active DR5
179 oligomers at the ERGIC, we asked how misfolded proteins and DR5 interact. Considering the
180 precedence that i) DR5 binds unstructured peptides mimicking TRAIL (Kajiwara et al. 2004;
181 Pavet et al. 2010) and ii) that UPR sensors can directly bind misfolded protein to sense ER
182 stress (Karagöz et al. 2017; Wang et al. 2018; Gardner and Walter 2011), we hypothesized that

DR5 may directly recognize unstructured regions of misfolded proteins through its ectodomain (ECD) that would project into the ERGIC lumen. Probing a peptide array with purified recombinant Fc-tagged DR5 ECD revealed promiscuous recognition of amino acid sequences throughout the ectodomain of MPZ and within extracellular loops of RHO (Fig 3A, Fig 3–figure supplement 1A-1B). Quantification of the relative signal intensity revealed that DR5-binding sequences were enriched for aliphatic and aromatic residues whereas polar and acidic residues were excluded (Fig 3–figure supplement 1C), reminiscent of qualities that become surface-exposed in misfolded or unfolded proteins.

To validate the specificity of DR5 interactions on the array, we performed pull-down assays on the MPZ-derived peptide exhibiting the strongest signal (spots C18-C19 in Fig 3A, hereon referred to as MPZ-ecto) with recombinant Fc-tagged DR5 ECD versus TNFR1 ECD as a selectivity control. The MPZ-ecto peptide bound specifically to the DR5 ECD but not the TNFR1 ECD (Fig 3B). Under equilibrium conditions, interaction with MPZ-ecto peptide quenched fluorescently labeled DR5 ECD but not fluorescently labeled TNFR1 ECD, yielding an apparent binding affinity of $K_{1/2}$ = 109 μM $\pm$ 11 μM with a Hill coefficient of 2.6 (Fig 3C, Fig 3–figure supplement 2A). Adding excess unlabeled DR5 ECD restored fluorescence (Fig 3–figure supplement 2B), indicating that the quenching reflected a specific and reversible interaction between the DR5 ECD and the MPZ-ecto peptide. Moreover, mutation of two aromatic amino acids (both Tyr) to disfavored acidic amino acids (Glu) abrogated binding (Fig 3C), demonstrating that the interaction is sequence-specific.

The Hill coefficient of 2.6 suggested cooperative binding. Therefore, we tested if the DR5 ECD forms oligomers in the presence of peptide. In the absence of peptide, the addition of a chemical cross-linker captured dimers of FLAG-tagged DR5 ECD (Fig 3D, Fig 3–figure supplement 2C), consistent with pre-ligand assembled dimers previously observed for members of the TNFR family (Clancy et al. 2005; Siegel et al. 2000; Chan et al. 2000) . With increasing concentration of peptide (up to 200 μM), crosslinking revealed multimers of the DR5 ECD (Fig

3D), indicating that the peptide acts as a ligand to template assembly of DR5 oligomers. Interestingly, excess peptide (400 μM) dissociated higher-order oligomers of DR5, suggesting a lower valency of interaction when the DR5 concentration becomes limiting.

To examine the DR5 oligomerization at saturating peptide concentrations by an orthogonal method, we fractionated DR5 ECD-peptide complexes using size exclusion chromatography. At 100 μM MPZ-ecto (~$K_{1/2}$), DR5 ECD co-eluted with the peptide as higher-order oligomers near the void volume (7-8 ml) and as apo-dimers centered at 14 ml, as shown in the Coomassie blue-stained gel for DR5 and fluorescence scan for fluorescein-labeled MPZ-ecto peptide (Fig 3E-3F, green outline). This elution pattern was similar to that of the DR5 ECD-TRAIL complex, for which both proteins co-eluted near the void volume (Fig 3–figure supplement 2E-2F). However, with excess MPZ-ecto peptide at 400 μM (4-times $K_{1/2}$), the proportion of higher-order oligomers of DR5 ECD and the peptide diminished and re-distributed to later eluting fractions at 12-15 ml (Fig 3–figure supplement 2G-2H, teal outline), indicating disassembly into smaller oligomers of DR5 ECD and pointing at the reversibility of the higher-order DR5-peptide assemblies. Importantly, the non-binding peptide bearing the Tyr-to-Glu substitutions did not co-migrate with or induce the oligomerization of DR5 ECD (Fig 3E-3F, magenta outline).

Disrupting misfolded protein binding to DR5 attenuates ER stress-mediated apoptosis.

Since mutating the Tyr residues to Glu on the MPZ-ecto peptide proved sufficient to disrupt the DR5 ECD interaction in solution, we tested the ability of this minimal MPZ-derived sequence to bind to and activate DR5 in cells. To this end, we generated constructs that replaced the ectodomain of MPZ with either the MPZ-ecto peptide, the peptide sequence with Tyr-to-Glu substitutions, or the peptide with all its aromatic residues changed to Glu to further deplete DR5-favored amino acid side chains revealed in the peptide array (Fig 4A). In a titration of MPZ-ecto peptide expression, the WT peptide sequence induced more PARP cleavage and

caspase activity than similar or higher levels of the peptides containing Glu substitutions (Fig 4B, compare lanes 5, 7, and 10, Fig 4C). The Glu-containing peptides also induced reduced PARP cleavage in another epithelial cell type, HepG2 (Fig 4– figure supplement 1A). Acute knockdown of DR5 reduced PARP cleavage during MPZ-ecto peptide expression, while exogenous FLAG-tagged DR5 expression restored PARP cleavage (Fig 4–figure supplement 1B). Of note, depletion of DR5 resulted in detection of higher levels of the MPZ-ecto peptide, likely because cells with this protein-folding burden were not eliminated.

Expressing comparable levels of the MPZ-ecto peptide and its variants (using conditions of lanes 5, 7, and 10 in Fig 4B) induced *XBP1* mRNA splicing and transcription of CHOP and BiP mRNAs, indicating that the presence of these peptides perturb ER protein folding homeostasis to a similar degree (Fig 4D, Fig 4E). Immunofluorescence showed that the MPZ-ecto peptide localized to the plasma membrane and within intracellular puncta that partially overlapped with ERGIC signal, although to a lesser extent than overexpressed full-length MPZ (Fig 4F, Fig 4–figure supplement 2C). The Glu-containing mutant peptides were similarly distributed within cells with no significant difference in their average correlation with ERGIC signal (Fig 4–figure supplement 2A-2B). DR5, in all three conditions, also showed a positive correlation with the ERGIC marker (Fig 4–figure supplement 2E). To determine if DR5 interacted with the MPZ-ecto peptide or its mutants, we immunoprecipitated the GFP-tagged peptides. Pulldown of the MPZ-ecto peptide enriched for DR5 relative to the Glu-containing mutant peptides (Fig 4G, Fig 4–figure supplement 3A). Consistent with this specific enrichment of DR5 for the WT sequence, PARP cleavage and caspase activity measured in cell lysates were increased with the WT MPZ-ecto relative to the mutants (Fig 4B-4C). To confirm that the expression of MPZ-ecto peptide induces apoptotic cell death, we measured annexin V staining in the absence and presence of the pan-caspase inhibitor z-VAD (Fig 4H, Figure 4–figure supplement 2C-2D). As expected, expressing the MPZ-ecto peptide increased annexin V staining relative to the empty vector but treatment with zVAD diminished the extent of annexin

V staining (Fig 4H). Importantly, cells expressing the Glu-containing mutant peptides exhibit decreased annexin V staining, demonstrating that DR5 binding of exposed polypeptides on misfolded protein is important for driving apoptosis.

Discussion

Our data identify misfolded protein as the ER stress factor that switches upregulated DR5 from its inactive auto-inhibited dimer state to active multimeric clusters to initiate DISC assembly and apoptosis at the ER-Golgi intermediate complex. We have examined the mechanism of apoptosis induction by the sustained expression of three different candidate ER-trafficked proteins associated with CHOP-dependent disease pathologies: MPZ, RHO, and INS (Pennuto et al. 2008; W. C. Chiang et al. 2016; Oyadomari et al. 2002). In epithelial cells, overexpression of each protein induces apoptosis in a DR5-dependent manner. Consistent with previous reports of ectopic CHOP expression in the absence of ER stress (McCullough et al. 2001; Han et al. 2013; Southwood et al. 2016), CHOP-driven upregulation of DR5 alone did not account for the apoptosis observed during the overexpression of an ER-trafficked protein. For MPZ and RHO, the intracellular, misfolded pools of each protein physically associated with the DR5-caspase 8 complex. For proinsulin, which weakly associated with DR5 but triggered apoptosis to a similar extent, we believe it is likely that overexpression of this singular protein perturbed the folding of endogenous trafficking substrates and thereby provided other, perhaps more favored, misfolding substrates to directly engage DR5. This latter scenario is likely to occur under pharmacologically induced ER stress as well. The interaction between misfolded protein and DR5 bridges the long-standing mechanistic gap of why CHOP expression (and subsequent upregulation of its downstream factors) is necessary but not sufficient to drive cell death. Through characterizing the interaction between the DR5 ECD and peptide sequences of ER-trafficked proteins, we demonstrate that DR5 promiscuously binds to exposed hydrophobic

stretches of misfolded proteins with an affinity in the range of 100 μM and in a highly cooperative manner.

To grasp how such a high concentration of misfolded protein could occur in the ERGIC, it is important to consider that the compartment is composed of vesicles and tubules measuring 60-100 nm in diameter and <500 nm in length. In a back-of-the-envelope calculation, we estimate that reaching 100 μM in a vesicle with a diameter of 100 nm would require only 32 molecules (Sesso et al. 1994; Fan, Roth, and Zuber 2003). The measured affinities are therefore well within physiological range. Quantitative fluorescence microscopy of living COS7 cells has indicated up to 100 molecules of a GFP-tagged viral glycoprotein in a 100-nm vesicle (Hirschberg et al. 1998), providing experimental evidence that surpassing concentrations of 100 μM is indeed physiologically relevant. In fact, the “low” affinity between DR5 and misfolded proteins is likely a necessary feature that prevents aberrant DR5 oligomerization and activation in the crowded lumenal environment of membrane-bound compartments, as we previously established for other unfolded protein sensors, such as IRE1 (Gardner et al. 2013; Gardner and Walter 2011; Karagöz et al. 2017).

Given that misfolded receptors can be exported from the ER when quality control mechanisms are overwhelmed (Satpute-Krishnan et al. 2014; Sirkis, Aparicio, and Schekman 2017), detection of misfolded proteins by DR5 downstream of the ER likely serves to prevent the cell from displaying or secreting dysfunctional proteins that would be detrimental in a multicellular context. While IRE1 and PERK act as initial UPR sensors in the ER, DR5 acts as a late sensor of misfolded protein at the ERGIC during unmitigated ER stress. Thus, intracellular DR5 triggers apoptosis to enforce a terminal quality control checkpoint for secretory and transmembrane proteins. We postulate that other members of the TNFR family, e.g. DR4, which has been reported to play a role in cell death during Golgi stress (van Raam et al. 2017), may respond similarly to intracellular stimuli.

Although extensive research has focused on the therapeutic activation of death

receptors including DR5 (Avi Ashkenazi 2015), limited strategies exist to inhibit such receptors despite their demonstrated role in apoptosis-mediated disease progression (Vunnam et al. 2017). Namely, DR5-mediated apoptosis in hepatocytes has been linked to non-alcoholic fatty liver disease, while CHOP-dependent apoptosis in Schwann cells—wherein a role for DR5 has yet to be investigated—may contribute to diabetic peripheral neuropathies (Cazanave et al. 2011; Sato et al. 2015). Our finding that the assembly and disassembly of DR5 ECD oligomers can be controlled by a peptide raises the possibility that intracellular DR5 activation could be inhibited through small molecule ligand-induced dissociation of DR5 clusters to prevent apoptosis and thus preserve cell viability in the face of unresolved ER stress. From the work herein, this notion now emerges as a promising strategy to interfere therapeutically with deleterious death receptor function.

References

Ashkenazi, A, and V M Dixit. 1998. “Death Receptors: Signaling and Modulation.” *Science (New York, N.Y.)* 281 (5381). American Association for the Advancement of Science: 1305–8. https://doi.org/10.1126/SCIENCE.281.5381.1305.

Ashkenazi, Avi. 2015. “Targeting the Extrinsic Apoptotic Pathway in Cancer: Lessons Learned and Future Directions.” *The Journal of Clinical Investigation* 125 (2). American Society for Clinical Investigation: 487–89. https://doi.org/10.1172/JCI80420.

Carpenter, Anne E, Thouis R Jones, Michael R Lamprecht, Colin Clarke, In Kang, Ola Friman, David A Guertin, et al. 2006. “CellProfiler: Image Analysis Software for Identifying and Quantifying Cell Phenotypes.” *Genome Biology* 7 (10): R100. https://doi.org/10.1186/gb-2006-7-10-r100.

Cazanave, Sophie C, Justin L Mott, Steven F Bronk, Nathan W Werneburg, Christian D Fingas, X Wei Meng, Niklas Finnberg, Wafik S El-Deiry, Scott H Kaufmann, and Gregory J Gores. 2011. “Death Receptor 5 Signaling Promotes Hepatocyte Lipoapoptosis.” *The Journal of Biological Chemistry* 286 (45). American Society for Biochemistry and Molecular Biology: 39336–48. https://doi.org/10.1074/jbc.M111.280420.

Chan, F K, H J Chun, L Zheng, R M Siegel, K L Bui, and M J Lenardo. 2000. “A Domain in TNF Receptors That Mediates Ligand-Independent Receptor Assembly and Signaling.” *Science (New York, N.Y.)* 288 (5475): 2351–54. http://www.ncbi.nlm.nih.gov/pubmed/10875917.

Chang, Tsun-Kai, David A. Lawrence, Min Lu, Jenille Tan, Jonathan M. Harnoss, Scot A. Marsters, Peter Liu, Wendy Sandoval, Scott E. Martin, and Avi Ashkenazi. 2018. “Coordination between Two Branches of the Unfolded Protein Response Determines Apoptotic Cell Fate.” *Molecular Cell* 71 (4). Cell Press: 629–636.e5. https://doi.org/10.1016/J.MOLCEL.2018.06.038.

Chiang, Wei-Chieh, Victory Joseph, Douglas Yasumura, Michael T. Matthes, Alfred S. Lewin, Marina S. Gorbatyuk, Kelly Ahern, Matthew M. LaVail, and Jonathan H. Lin. 2016.

"Ablation of Chop Transiently Enhances Photoreceptor Survival but Does Not Prevent Retinal Degeneration in Transgenic Mice Expressing Human P23H Rhodopsin." In *Advances in Experimental Medicine and Biology*, 854:185–91. https://doi.org/10.1007/978-3-319-17121-0_25.

Chiang, Wei Chieh, Victory Joseph, Douglas Yasumura, Michael T. Matthes, Alfred S. Lewin, Marina S. Gorbatyuk, Kelly Ahern, Matthew M. Lavail, and Jonathan H. Lin. 2016. "Ablation of Chop Transiently Enhances Photoreceptor Survival but Does Not Prevent Retinal Degeneration in Transgenic Mice Expressing Human P23H Rhodopsin." In *Advances in Experimental Medicine and Biology*, 854:185–91. Springer New York LLC. https://doi.org/10.1007/978-3-319-17121-0_25.

Clancy, Lauren, Karen Mruk, Kristina Archer, Melissa Woelfel, Juthathip Mongkolsapaya, Gavin Screaton, Michael J Lenardo, and Francis Ka-Ming Chan. 2005. "Preligand Assembly Domain-Mediated Ligand-Independent Association between TRAIL Receptor 4 (TR4) and TR2 Regulates TRAIL-Induced Apoptosis." *Proceedings of the National Academy of Sciences of the United States of America* 102 (50): 18099–104. https://doi.org/10.1073/pnas.0507329102.

Dickens, Laura S., Robert S. Boyd, Rebekah Jukes-Jones, Michelle A. Hughes, Gemma L. Robinson, Louise Fairall, John W.R. Schwabe, Kelvin Cain, and Marion MacFarlane. 2012. "A Death Effector Domain Chain DISC Model Reveals a Crucial Role for Caspase-8 Chain Assembly in Mediating Apoptotic Cell Death." *Molecular Cell* 47 (2). Cell Press: 291–305. https://doi.org/10.1016/J.MOLCEL.2012.05.004.

Dufour, Florent, Thibault Rattier, Andrei Alexandru Constantinescu, Luciana Zischler, Aymeric Morlé, Hazem Ben Mabrouk, Etienne Humblin, et al. 2017. "TRAIL Receptor Gene Editing Unveils TRAIL-R1 as a Master Player of Apoptosis Induced by TRAIL and ER Stress." *Oncotarget* 8 (6): 9974–85. https://doi.org/10.18632/oncotarget.14285.

Fan, Jing-Yu, J[illegible]rgen Roth, and Christian Zuber. 2003. "Ultrastructural Analysis of Transitional

376 Endoplasmic Reticulum and Pre-Golgi Intermediates: A Highway for Cars and Trucks."
377 *Histochemistry and Cell Biology* 120 (6). Springer-Verlag: 455–63.
378 https://doi.org/10.1007/s00418-003-0597-1.
379 Gardner, B. M., D. Pincus, K. Gotthardt, C. M. Gallagher, and P. Walter. 2013. "Endoplasmic
380 Reticulum Stress Sensing in the Unfolded Protein Response." *Cold Spring Harbor*
381 *Perspectives in Biology* 5 (3): a013169–a013169.
382 https://doi.org/10.1101/cshperspect.a013169.
383 Gardner, B. M., and P. Walter. 2011. "Unfolded Proteins Are Ire1-Activating Ligands That
384 Directly Induce the Unfolded Protein Response." *Science* 333 (6051): 1891–94.
385 https://doi.org/10.1126/science.1209126.
386 Han, Jaeseok, Sung Hoon Back, Junguk Hur, Yu-Hsuan Lin, Robert Gildersleeve, Jixiu Shan,
387 Celvie L. Yuan, et al. 2013. "ER-Stress-Induced Transcriptional Regulation Increases
388 Protein Synthesis Leading to Cell Death." *Nature Cell Biology* 15 (5). Nature Publishing
389 Group: 481–90. https://doi.org/10.1038/ncb2738.
390 Harding, Heather P, Yuhong Zhang, Huiquing Zeng, Isabel Novoa, Phoebe D Lu, Marcella
391 Calfon, Navid Sadri, et al. 2003. "An Integrated Stress Response Regulates Amino Acid
392 Metabolism and Resistance to Oxidative Stress." *Molecular Cell* 11 (3): 619–33.
393 http://www.ncbi.nlm.nih.gov/pubmed/12667446.
394 Hirschberg, K, C M Miller, J Ellenberg, J F Presley, E D Siggia, R D Phair, and J Lippincott-
395 Schwartz. 1998. "Kinetic Analysis of Secretory Protein Traffic and Characterization of Golgi
396 to Plasma Membrane Transport Intermediates in Living Cells." *The Journal of Cell Biology*
397 143 (6). The Rockefeller University Press: 1485–1503.
398 https://doi.org/10.1083/jcb.143.6.1485.
399 Hughes, Michelle A., Claudia Langlais, Kelvin Cain, and Marion MacFarlane. 2013. "Isolation,
400 Characterisation and Reconstitution of Cell Death Signalling Complexes." *Methods* 61 (2).
401 Academic Press: 98–104. https://doi.org/10.1016/J.YMETH.2013.02.006.

Hymowitz, Sarah G., Hans W. Christinger, Germaine Fuh, Mark Ultsch, Mark O'Connell, Robert F. Kelley, Avi Ashkenazi, and Abraham M. De Vos. 1999. "Triggering Cell Death: The Crystal Structure of Apo2L/TRAIL in a Complex with Death Receptor 5." *Molecular Cell* 4 (4). Cell Press: 563–71. https://doi.org/10.1016/S1097-2765(00)80207-5.

Iurlaro, Raffaella, Franziska Püschel, Clara Lucía León-Annicchiarico, Hazel O'Connor, Seamus J Martin, Daniel Palou-Gramón, Estefanía Lucendo, and Cristina Muñoz-Pinedo. 2017. "Glucose Deprivation Induces ATF4-Mediated Apoptosis through TRAIL Death Receptors." *Molecular and Cellular Biology* 37 (10): e00479-16. https://doi.org/10.1128/MCB.00479-16.

Jin, Zhaoyu, Yun Li, Robert Pitti, David Lawrence, Victoria C. Pham, Jennie R. Lill, and Avi Ashkenazi. 2009. "Cullin3-Based Polyubiquitination and p62-Dependent Aggregation of Caspase-8 Mediate Extrinsic Apoptosis Signaling." *Cell* 137 (4). Cell Press: 721–35. https://doi.org/10.1016/J.CELL.2009.03.015.

Kajiwara, Kazumi, Atsuhiro Saito, Shin-ichi Ogata, and Masao Tanihara. 2004. "Synthetic Peptides Corresponding to Ligand-Binding Region of Death Receptors, DR5, Fas, and TNFR, Specifically Inhibit Cell Death Mediated by the Death Ligands, Respectively." *Biochimica et Biophysica Acta (BBA) - Proteins and Proteomics* 1699 (1–2): 131–37. https://doi.org/10.1016/j.bbapap.2004.02.016.

Karagöz, G Elif, Diego Acosta-Alvear, Hieu T Nguyen, Crystal P Lee, Feixia Chu, and Peter Walter. 2017. "An Unfolded Protein-Induced Conformational Switch Activates Mammalian IRE1." *eLife* 6 (October). eLife Sciences Publications, Ltd. https://doi.org/10.7554/eLife.30700.

Kischkel, F C, D A Lawrence, A Chuntharapai, P Schow, K J Kim, and A Ashkenazi. 2000. "Apo2L/TRAIL-Dependent Recruitment of Endogenous FADD and Caspase-8 to Death Receptors 4 and 5." *Immunity* 12 (6): 611–20. http://www.ncbi.nlm.nih.gov/pubmed/10894161.

Lam, Mable, David A Lawrence, Avi Ashkenazi, and Peter Walter. 2018. "Confirming a Critical

Role for Death Receptor 5 and Caspase-8 in Apoptosis Induction by Endoplasmic Reticulum Stress." *Cell Death and Differentiation* 25 (8): 1530–31. https://doi.org/10.1038/s41418-018-0155-y.

LeBlanc, Heidi, David Lawrence, Eugene Varfolomeev, Klara Totpal, John Morlan, Peter Schow, Sharon Fong, Ralph Schwall, Dominick Sinicropi, and Avi Ashkenazi. 2002. "Tumor-Cell Resistance to Death Receptor–induced Apoptosis through Mutational Inactivation of the Proapoptotic Bcl-2 Homolog Bax." *Nature Medicine* 8 (3). Nature Publishing Group: 274–81. https://doi.org/10.1038/nm0302-274.

Lu, M., D. A. Lawrence, S. Marsters, D. Acosta-Alvear, P. Kimmig, A. S. Mendez, A. W. Paton, J. C. Paton, P. Walter, and A. Ashkenazi. 2014. "Opposing Unfolded-Protein-Response Signals Converge on Death Receptor 5 to Control Apoptosis." *Science* 345 (6192): 98–101. https://doi.org/10.1126/science.1254312.

McCullough, K D, J L Martindale, L O Klotz, T Y Aw, and N J Holbrook. 2001. "Gadd153 Sensitizes Cells to Endoplasmic Reticulum Stress by down-Regulating Bcl2 and Perturbing the Cellular Redox State." *Molecular and Cellular Biology* 21 (4): 1249–59. https://doi.org/10.1128/MCB.21.4.1249-1259.2001.

Mongkolsapaya, Juthathip, Jonathan M. Grimes, Nan Chen, Xiao Ning Xu, David I. Stuart, E. Yvonne Jones, and Gavin R. Screaton. 1999. "Structure of the TRAIL-DR5 Complex Reveals Mechanisms Conferring Specificity in Apoptotic Initiation." *Nature Structural Biology* 6 (11): 1048–53. https://doi.org/10.1038/14935.

Muzio, Marta, Brent R. Stockwell, Henning R. Stennicke, Guy S. Salvesen, and Vishva M. Dixit. 1998. "An Induced Proximity Model for Caspase-8 Activation." *Journal of Biological Chemistry* 273 (5): 2926–30. https://doi.org/10.1074/jbc.273.5.2926.

Oyadomari, Seiichi, Akio Koizumi, Kiyoshi Takeda, Tomomi Gotoh, Shizuo Akira, Eiichi Araki, and Masataka Mori. 2002. "Targeted Disruption of the Chop Gene Delays Endoplasmic Reticulum Stress–mediated Diabetes." *Journal of Clinical Investigation* 109 (4): 525–32.

https://doi.org/10.1172/JCI14550.

Pan, Liqiang, Tian-Min Fu, Wenbin Zhao, Linlin Zhao, Wen Chen, Chixiao Qiu, Wenhui Liu, et al. 2019. “Higher-Order Clustering of the Transmembrane Anchor of DR5 Drives Signaling.” *Cell* 0 (0). Elsevier. https://doi.org/10.1016/j.cell.2019.02.001.

Pavet, V., J. Beyrath, C. Pardin, A. Morizot, M.-C. Lechner, J.-P. Briand, M. Wendland, et al. 2010. “Multivalent DR5 Peptides Activate the TRAIL Death Pathway and Exert Tumoricidal Activity.” *Cancer Research* 70 (3): 1101–10. https://doi.org/10.1158/0008-5472.CAN-09-2889.

Pennuto, Maria, Elisa Tinelli, MariaChiara Malaguti, Ubaldo Del Carro, Maurizio D’Antonio, David Ron, Angelo Quattrini, M. Laura Feltri, and Lawrence Wrabetz. 2008. “Ablation of the UPR-Mediator CHOP Restores Motor Function and Reduces Demyelination in Charcot-Marie-Tooth 1B Mice.” *Neuron* 57 (3). Cell Press: 393–405. https://doi.org/10.1016/J.NEURON.2007.12.021.

Pitti, Robert M., Scot A. Marsters, Siegfried Ruppert, Christopher J. Donahue, Alison Moore, and Avi Ashkenazi. 1996. “Induction of Apoptosis by Apo-2 Ligand, a New Member of the Tumor Necrosis Factor Cytokine Family.” *Journal of Biological Chemistry* 271 (22): 12687–90. https://doi.org/10.1074/jbc.271.22.12687.

Raam, Bram J van, Tamara Lacina, Ralph K Lindemann, and Jan H Reiling. 2017. “Secretory Stressors Induce Intracellular Death Receptor Accumulation to Control Apoptosis.” *Cell Death & Disease* 8 (10): e3069. https://doi.org/10.1038/cddis.2017.466.

Sato, Keisuke, Ryosuke Tatsunami, Kaori Yama, Yu Murao, and Yoshiko Tampo. 2015. “Glycolaldehyde Induces Endoplasmic Reticulum Stress and Apoptosis in Schwann Cells.” *Toxicology Reports* 2 (January). Elsevier: 1454–62. https://doi.org/10.1016/J.TOXREP.2015.10.014.

Satpute-Krishnan, Prasanna, Monica Ajinkya, Savithri Bhat, Eisuke Itakura, Ramanujan S. Hegde, and Jennifer Lippincott-Schwartz. 2014. “ER Stress-Induced Clearance of

Misfolded GPI-Anchored Proteins via the Secretory Pathway." *Cell* 158 (3): 522–33. https://doi.org/10.1016/j.cell.2014.06.026.

Sesso, A, F P de Faria, E S Iwamura, and H Corrêa. 1994. "A Three-Dimensional Reconstruction Study of the Rough ER-Golgi Interface in Serial Thin Sections of the Pancreatic Acinar Cell of the Rat." *Journal of Cell Science* 107 (Pt 3) (March): 517–28. http://www.ncbi.nlm.nih.gov/pubmed/8006070.

Sheridan, J P, S A Marsters, R M Pitti, A Gurney, M Skubatch, D Baldwin, L Ramakrishnan, et al. 1997. "Control of TRAIL-Induced Apoptosis by a Family of Signaling and Decoy Receptors." *Science (New York, N.Y.)* 277 (5327): 818–21. http://www.ncbi.nlm.nih.gov/pubmed/9242611.

Siegel, R M, J K Frederiksen, D A Zacharias, F K Chan, M Johnson, D Lynch, R Y Tsien, and M J Lenardo. 2000. "Fas Preassociation Required for Apoptosis Signaling and Dominant Inhibition by Pathogenic Mutations." *Science (New York, N.Y.)* 288 (5475): 2354–57. http://www.ncbi.nlm.nih.gov/pubmed/10875918.

Sirkis, Daniel W, Renan E Aparicio, and Randy Schekman. 2017. "Neurodegeneration-Associated Mutant TREM2 Proteins Abortively Cycle between the ER and ER-Golgi Intermediate Compartment." *Molecular Biology of the Cell* 28 (20): 2723–33. https://doi.org/10.1091/mbc.E17-06-0423.

Southwood, Cherie M., Bozena Fykkolodziej, Kathleen J. Maheras, Danielle M. Garshott, Molly Estill, Andrew M. Fribley, and Alexander Gow. 2016. "Overexpression of CHOP in Myelinating Cells Does Not Confer a Significant Phenotype under Normal or Metabolic Stress Conditions." *The Journal of Neuroscience* 36 (25): 6803–19. https://doi.org/10.1523/JNEUROSCI.1118-15.2016.

Spierings, Diana C., Elisabeth G. de Vries, Edo Vellenga, Fiona A. van den Heuvel, Jan J. Koornstra, Jelle Wesseling, Harry Hollema, and Steven de Jong. 2004. "Tissue Distribution of the Death Ligand TRAIL and Its Receptors." *Journal of Histochemistry & Cytochemistry*

52 (6): 821–31. https://doi.org/10.1369/jhc.3A6112.2004.

Sprick, M R, M A Weigand, E Rieser, C T Rauch, P Juo, J Blenis, P H Krammer, and H Walczak. 2000. “FADD/MORT1 and Caspase-8 Are Recruited to TRAIL Receptors 1 and 2 and Are Essential for Apoptosis Mediated by TRAIL Receptor 2.” *Immunity* 12 (6): 599–609. http://www.ncbi.nlm.nih.gov/pubmed/10894160.

Tabas, Ira, and David Ron. 2011. “Integrating the Mechanisms of Apoptosis Induced by Endoplasmic Reticulum Stress.” *Nature Cell Biology* 13 (3): 184–90. https://doi.org/10.1038/ncb0311-184.

Valley, Christopher C., Andrew K. Lewis, Deepti J. Mudaliar, Jason D. Perlmutter, Anthony R. Braun, Christine B. Karim, David D. Thomas, Jonathan R. Brody, and Jonathan N. Sachs. 2012. “Tumor Necrosis Factor-Related Apoptosis-Inducing Ligand (TRAIL) Induces Death Receptor 5 Networks That Are Highly Organized.” *Journal of Biological Chemistry* 287 (25): 21265–78. https://doi.org/10.1074/jbc.M111.306480.

Vanamee, Éva S, and Denise L Faustman. 2018. “Structural Principles of Tumor Necrosis Factor Superfamily Signaling.” *Science Signaling* 11 (511). American Association for the Advancement of Science: eaao4910. https://doi.org/10.1126/scisignal.aao4910.

Vunnam, Nagamani, Chih Hung Lo, Benjamin D. Grant, David D. Thomas, and Jonathan N. Sachs. 2017. “Soluble Extracellular Domain of Death Receptor 5 Inhibits TRAIL-Induced Apoptosis by Disrupting Receptor–Receptor Interactions.” *Journal of Molecular Biology* 429 (19). Academic Press: 2943–53. https://doi.org/10.1016/J.JMB.2017.08.009.

Walczak, H., M A Degli-Esposti, R S Johnson, P J Smolak, J Y Waugh, N Boiani, M S Timour, et al. 1997. “TRAIL-R2: A Novel Apoptosis-Mediating Receptor for TRAIL.” *The EMBO Journal* 16 (17): 5386–97. https://doi.org/10.1093/emboj/16.17.5386.

Walter, P., and D. Ron. 2011. “The Unfolded Protein Response: From Stress Pathway to Homeostatic Regulation.” *Science* 334 (6059): 1081–86. https://doi.org/10.1126/science.1209038.

Wang, Peng, Jingzhi Li, Jiahui Tao, and Bingdong Sha. 2018. “The Luminal Domain of the ER Stress Sensor Protein PERK Binds Misfolded Proteins and Thereby Triggers PERK Oligomerization.” *Journal of Biological Chemistry* 293 (11): 4110–21. https://doi.org/10.1074/jbc.RA117.001294.

Wei, M. C., W. X. Zong, E. H.Y. Cheng, T. Lindsten, V. Panoutsakopoulou, A. J. Ross, K. A. Roth, G. R. Macgregor, C. B. Thompson, and S. J. Korsmeyer. 2001. “Proapoptotic BAX and BAK: A Requisite Gateway to Mitochondrial Dysfunction and Death.” *Science* 292 (5517): 727–30. https://doi.org/10.1126/science.1059108.

Wiley, Steven R., Ken Schooley, Pamela J. Smolak, Wenie S. Din, Chang Pin Huang, Jillian K. Nicholl, Grant R. Sutherland, et al. 1995. “Identification and Characterization of a New Member of the TNF Family That Induces Apoptosis.” *Immunity* 3 (6): 673–82. https://doi.org/10.1016/1074-7613(95)90057-8.

Xu, Daqian, Zheng Wang, Yuxue Zhang, Wei Jiang, Yi Pan, Bao-Liang Song, and Yan Chen. 2015. “PAQR3 Modulates Cholesterol Homeostasis by Anchoring Scap/SREBP Complex to the Golgi Apparatus.” *Nature Communications* 6 (1). Nature Publishing Group: 8100. https://doi.org/10.1038/ncomms9100.

Yamaguchi, Hirohito, and Hong-Gang Wang. 2004. “CHOP Is Involved in Endoplasmic Reticulum Stress-Induced Apoptosis by Enhancing DR5 Expression in Human Carcinoma Cells.” *The Journal of Biological Chemistry* 279 (44). American Society for Biochemistry and Molecular Biology: 45495–502. https://doi.org/10.1074/jbc.M406933200.

Figure Legends

Fig 1. Misfolded proteins induce DR5-dependent apoptosis and assemble DR5-caspase 8 signaling complexes.

A) Confocal images of epithelial cells HCT116 fixed 24 h post-transfection with 0.25-1.0 μg of a plasmid containing myelin protein zero (MPZ) tagged with a C-terminal monomeric EGFP or 1.0 μg of the empty vector showing MPZ-GFP fluorescence (green) and immunofluorescence with an antibody against DR5 (red) (scale bar = 5 μm).

B) Western blot of HCT116 cell lysates harvested 24 h post-transfection with a titration of MPZ-GFP plasmid or the empty vector (C8 = caspase 8, cC3 = cleaved caspase 3). p55 represents full-length, inactive C8; p43 indicates a C8 intermediate after release of the active p10 subunit, and p29 corresponds to the released p18 and p10 subunits.

C) Western blot of HCT116 cells transfected with siRNA against a non-targeting (Nt) control or DR5 (48 h) followed by the empty vector -/+ 100 nM thapsigargin (Tg), 1.0 μg MPZ-GFP, or cytosolic GFP (24 h; * denotes degradation products; L and S denote the long and short isoforms of DR5, respectively; FL and C denote full-length and cleaved PARP, respectively).

D) Average percent of annexin V staining for HCT116 cells transfected as described in C) from n = 3 biological replicates (error bars = SEM; * indicates $p < 0.05$; ns indicates $p = 0.46$ as analyzed by unpaired t-test with equal SD). See Fig 1–figure supplement 4D for gating.

E) Top: Caspase 8 activity in size exclusion chromatography fractions from lysates of HCT116 cells transfected with 1.0 μg MPZ-GFP or cytosolic GFP (24 h). Bottom: Size exclusion fractions were pooled according to dotted grid lines and immunoblotted for DR5 and GFP (* denotes degradation products).

F) Immunoprecipitation of GFP-tagged proteins from lysates of HCT116 transfected with MPZ-GFP, cytosolic GFP, or the empty vector (L and S denote the long and short isoforms of DR5, respectively). The percent of total DR5 recovered has been quantified in Figure 1–figure supplement 5C.

G) Fold change in caspase 8 activity relative to the empty vector control for beads with immunoprecipitated contents shown in Fig 1F (error bars = SEM for n = 3 biological replicates; * indicates p = 0.023 and ns indicates p = 0.83 as calculated by unpaired t-tests with equal SD).

Fig 1–source data 1: FCS files and quantification of Annexin V staining for MPZ-GFP

This zip archive contains FCS files from n = 3 biological replicates of HCT116 transfected with the conditions outlined in Fig 1D. The excel file contains the quantification of Annexin V staining exported frow FlowJo.

Fig 1–source data 2: Caspase glo 8 measurements for IP of MPZ-GFP vs GFP

This zip archive contains the measured luminescent units for caspase glo 8 activity shown in Figures 1G (IP beads) and Fig 1S3C (input lysates). Coomassie gels used to normalize lysate concentration are included as .tif files.

Fig 1–figure supplement 1: Sustained MPZ-GFP expression invokes a terminal, pro-apoptotic UPR at late time points.

A) qPCR for reverse-transcribed transcripts harvested from HCT116 cells transfected with 0.12-1.0 μg of a plasmid containing myelin protein zero (MPZ) tagged with a C-terminal monomeric EGFP or 1.0 μg of the empty vector for 24 h (n = 3 technical replicates, error bars = SD; * denotes $p < 0.05$ as analyzed by multiple t-tests with Holm-Sidak correction for multiple comparisons).

B) Quantification of the mean intensity for DR5 versus the mean intensity of intracellular MPZ-GFP per cell for HCT116 transfected with 0.25 μg (left) and 1.0 μg (right) of MPZ-GFP plasmid to show the correlation between DR5 and MPZ-GFP expression levels per cell. Intensity values given by CellProfiler algorithms were normalized to 0.02 for DR5 and 0.06 for MPZ-GFP to assign arbitrary values. P values were calculated from unpaired two-tailed t-tests.

C) RT-PCR for unspliced and spliced forms of *Xbp1* mRNA isolated from HCT116 cells transfected for 24 h with the empty vector or for various time points with 1 μg MPZ-GFP, followed by cells treated with 100 nM Tg for 2 h and 24 h.

D) Western blot of HCT116 cell lysates harvested 24 h post-transfection with the empty vector, or 3-24 h post-transfection with 1 μg MPZ-GFP.

E) Fold change in caspase 8 activity, as measured by a luminescent caspase 8 substrate, of lysates from HCT116 harvested 3-24 h post-transfection with 1 μg MPZ-GFP relative to cells transfected with the empty vector control (error bars represent SD of n = 3 technical replicates; *** denotes $p < 0.005$, and ns indicates $p = 0.15$ by unpaired t-test with equal SD).

Fig 1–source data 3: qPCR analysis of MPZ-GFP titration

This zip archive contains the compiled excel file for qPCR data shown in Fig 1–figure supplement 1A along with the Prism 6 file used to perform multiple t-tests with Holm-Sidak correction for multiple comparisons

Fig 1–source data 4: Caspase glo 8 measurements for time course of MPZ-GFP transfection

This zip archive contains the measured luminescent units for caspase glo 8 activity shown in Figures 1–figure supplement 1E and the tif file of the Coomassie blue-stained gel used to normalize lysate concentrations.

Fig 1–figure supplement 2: Upregulating DR5 levels in the absence of ER stress through ectopic expression of CHOP is not sufficient to induce apoptosis.

A) Western blot of HCT116 cell lysates harvested 24 h post-transfection with a titration of 0.03-0.50 μg of a CHOP expression vector, 1 μg MPZ-GFP plasmid, or the empty vector (FL = full-length, C = cleaved).

B) qPCR for reverse-transcribed transcripts harvested from HCT116 cells transfected with 0.03-0.50 μg of a CHOP expression vector, 1.0 μg of MPZ-GFP, or 1.0 μg of the empty vector for 24 h (n = 3 technical replicates, error bars = SD, * denotes $p < 0.05$).

C) Representative images of automated counting for Trypan blue-stained cells, where green outlines denote non-stained (live) cells and red outlines denote stained cells (Trypan blue+, dead).

D) Average percentage of cells transfected as described in (S3A) stained with Trypan blue as quantified by automated cell counting from n = 3 biological replicates (error bars = SEM; ** denotes $p = 0.008$ and ns = non-significant for unpaired t-test with equal SD; ns[1] refers to $p = 0.19$ from unpaired t-test with Welch's correction for variance).

Fig 1–source data 5: qPCR and cell death measurement for CHOP expression

This zip archive contains the qPCR analysis from CHOP expression in Fig 1–figure supplement 2B, and brightfield images of Trypan Blue staining measured on the Countess II for n = 3 biological replicates, summarized in Fig 1–figure supplement 2D.

Fig 1–figure supplement 3: DR5 immunoprecipitates with FADD and MPZ-GFP.

A) Immunoprecipitation of DR5 from HCT116 transfected with MPZ-GFP or the empty vector and blotted for DR5, MPZ-GFP, and FADD.

B) Inputs for GFP pulldown performed in Fig. 1F.

C) Caspase 8 activity of inputs relative to the empty vector control for the GFP pulldown performed in Fig 1F (n = 3 biological replicates, error bars = SEM, ** indicates p = 0.0046, and * indicates $p < 0.05$ from unpaired t-tests with equal SD). Source data can be found in Figure 1–source data 2.

Fig 1–figure supplement 4: Sustained overexpression of other ER-trafficked proteins induce UPR-mediated apoptosis in a DR5-dependent manner.

A) qPCR for reverse-transcribed transcripts harvested from HCT116 cells transfected with 1.0 μg of GFP-tagged rhodopsin (RHO), proinsulin (INS), or 1.0 μg of the empty vector for 24 h (n = 2 biological replicates, each with 3 technical replicates; error bars = SD; * denotes $p < 0.05$).

B) RT-PCR for unspliced and spliced forms of *Xbp1* mRNA isolated from HCT116 cells transfected for 24 h with 1 μg of empty vector -/+ 100 nM Tg for 2 h, MPZ-GFP, INS-GFP, or RHO-GFP.

C) Western blot of HCT116 cells transfected with siRNA against a non-targeting (Nt) control or DR5 (48 h) followed by 1.0 μg RHO-GFP or INS-GFP (24 h).

D) Representative flow cytometry histograms of HCT116 cells transfected with the listed siRNA and vector and stained with annexin V-AlexaFluor647. Y-axis has been scaled so that the mode = 100%. Dotted lines represent gating to distinguish staining-positive cells. Left: Histograms of fluorescence at 647 nm to measure annexin V staining. Right: Histograms of fluorescence at 488 nm to compare level and distribution of GFP-tagged protein expression. To note, GFP expression profiles for the same construct are similar between different siRNA transfected samples.

E) Average percent of Annexin V-positive cells for HCT116 cells transfected with siRNA and GFP-tagged rhodopsin/proinsulin (n = 3 biological replicates, error bars = SEM, * indicates $p = 0.011$, ** indicates $p = 0.005$ from unpaired t-test with equal SD). Gating for annexin V-positive staining is shown in Fig 1–figure supplement 4D.

Fig 1–source data 6: qPCR analysis of INS and RHO-GFP expression

This zip archive contains the compiled excel file for qPCR data shown in Fig 1–figure supplement 4A along with the Prism 6 file used to perform multiple t-tests with Holm-Sidak correction for multiple comparisons.

Fig 1–source data 7: FCS files and quantification of Annexin V staining for INS and RHO

This zip archive contains FCS files from n = 3 biological replicates of HCT116 transfected with the conditions outlined in Fig 1–figure supplement 4E. The excel file contains the quantification of annexin V staining exported frow FlowJo.

Fig 1–figure supplement 5: DR5 engages a selective subset of ER-trafficked client proteins upon prolonged ER stress.

A) Pulldown of GFP-tagged proteins from HCT116 transfected with INS, RHO, or cytosolic GFP. Inputs (left) and immunoprecipitated samples (right) were immunoblotted for GFP and DR5 (L and S indicate long and short isoforms, respectively).

B) Fold change in caspase 8 activity relative to cytosolic GFP for beads with immunoprecipitated contents described in Fig 1–figure supplement 5A as measured by caspase glo 8 luminescence (n = 2 biological replicates, error bars = SEM, * indicates $p < 0.05$, ** indicates $p = 0.0013$, **** indicates $p < 0.005$ from unpaired t-tests with equal SD).

C) Quantification of the percent of total DR5 recovered in the IPs of GFP-tagged proteins, shown in Fig 1G and Figure 1–figure supplement 5A. (n = 3 biological replicates for GFP and MPZ, while n = 2 biological replicates for INS and RHO. * denotes $p = 0.016$, ** denotes $p = 0.0035$, and ns denotes $p = 0.39$ from unpaired t-test with equal SD) The DR5 signal of the input and IP lanes were quantified from the same exposure and then normalized to the amount loaded on the gel. Source data of blots and quantification are provided in Fig 1–source data 9.

Fig 1–source data 8: Caspase glo 8 measurements for IP of INS and RHO-GFP

This zip archive contains the measured luminescent units for caspase glo 8 activity shown in Figures 1S5B (input lysates and IP beads). Coomassie gels used to normalize lysate concentration are included as .tif files.

Fig 1–source data 9: Westerns and quantification of DR5 recovered on IPs

This zip archive contains images of the Western blots and measurements used to quantify the amount of DR5 in the IP samples relative to the input lysate

Fig 2: Misfolded protein engages DR5 at the ER-Golgi intermediate compartment, inducing active DR5 signaling clusters.

A) Top: Immunofluorescence of HCT116 cells transfected with MPZ-GFP (green) for 24 h and stained with anti-DR5 (red, scale bar 5 μm). Bottom: Enlargements of the inset stepping through the z-plane in 0.5 μm increments (scale bar 2 μm).

B) Subcellular fractionation of lysate expressing MPZ-GFP, where IRE1 marks the ER, Giantin marks the Golgi, Sec31A and Sec23A mark COPII vesicles, and ERGIC53 and RCAS1 correspond to ER-Golgi intermediate compartment. Bands of the expected size are indicated by "–" and bands that may represent a modified or degraded protein are indicated by *.

C) Average caspase activity of each fraction from subcellular gradient centrifugation in (B) normalized to total lysate (input) measured by caspase 8 substrate luminescence (n = 3 biological replicates, error bars = SEM; ns[1] indicates p = 0.079, * denotes p = 0.015, and ns indicates p = 0.31 from unpaired t-tests with equal SD).

D) Top: Immunostaining of DR5 and ERGIC53 in fixed HCT116 cells transfected with MPZ-GFP for 24 h as in (A). Bottom: Merged images with ERGIC53 in magenta or cyan to depict overlapping signal as white (scale bar = 5 μm, insets scale bar = 2 μm).

E) Immunostaining of DR5 and giantin in fixed HCT116 cells expressing MPZ-GFP. Giantin is magenta in the overlay with MPZ (green) or cyan in the overlay with DR5 (red). Bottom row enlarges the inset marked in the merges images to show little overlapping signal with Giantin (scale bar = 5 μm, inset scale bar = 1 μm).

F) Box-whisker plots quantifying the Pearson's correlation per cell between DR5 and ERGIC53 (mean = 0.61 ± 0.03) or Giantin (mean = 0.14 ± 0.02) within MPZ-positive cells (N > 55), where whiskers correspond to minimum and maximum values of the data (**** indicates p < 0.001).

Fig 2–source data 1: Caspase activity for fractions of iodixanol gradient

This excel file contains the caspase glo 8 luminescent units of the fractionation samples (n = 3 biological replicates) shown in Fig 2C.

Fig 2–figure supplement 1: Intracellular puncta of overexpressed MPZ and rhodopsin proteins show significant co-localization with DR5 clusters.

A) Immunofluorescence of fixed HCT116 cells transfected with siRNA (left: non-targeting, right: siDR5) for 48 h and MPZ-GFP (green in merge) for 24 h and subsequently immunostained for anti-DR5 (red in merge). Two representative confocal images are shown for each siRNA treatment, where the scale bar corresponds to 5 μm.

B) Immunofluorescence of fixed HCT116 cells expressing RHO-GFP for 24 h and stained for DR5 and GFP (scale bar = 5 μm, inset scale bar = 2 μm).

C) Quantification of Pearson's correlation per cell between DR5 signal and ER-trafficked protein (MPZ and RHO) 24 h-post transfection from original image files versus artificially rotated image files, for which the GFP channel was rotated 90^{o} with respect to the other channel. Whisker-box plots depict the Tukey method**.** Statistics were performed through unpaired two-tailed t-tests, where **** indicates $p < 0.0001$ and the variance was non-significant.

D) Immunofluorescence for DR5 and RCAS1 in fixed HCT116 cells expressing MPZ-GFP. RCAS1 is magenta in the overlay with MPZ (green) or cyan in the overlay with DR5 (red), where white puncta signify co-localized signal (scale bar = 5 μm, inset scale bar = 1 μm).

Fig 2–figure supplement 2: Misfolded protein accumulation in the ERGIC precedes DR5 retention in the ERGIC.

A) Immunofluorescence for DR5 and ERGIC53 in HCT116 fixed 20 hr post-transfection. ERGIC53 is magenta in the overlay with MPZ (green) or cyan in the overlay with DR5 (red) (scale bar = 5 μm). Arrows in inset images depict regions where MPZ and ERGIC53 signal overlap (scale bar = 2 μm).

B) Quantification of Pearson's correlation per cell between ERGIC and MPZ, or Giantin and MPZ of fixed HCT116 cells at the specified time after MPZ-GFP transfection. Whisker-box plots depict the Tukey method**.** Statistics were performed through unpaired two-tailed t-tests, where **** indicates p< 0.001 and ns means not significant, and the variance was non-significant.

C) Quantification of Pearson's correlation per cell between DR5 signal and ERGIC53 of fixed HCT116 cells at 20 h and 24 h post-transfection with MPZ-GFP. Whisker-box plots depict the Tukey method**.** Statistics were performed through unpaired two-tailed t-tests, where **** indicates p< 0.001 and the variance was non-significant.

Fig 3: Direct binding of exposed ER-trafficked protein sequences to the DR5 ECD is sufficient to induce oligomerization.

A) A peptide array tiled with sequences from the ectodomain of myelin protein zero (MPZ) and extracellular loops from rhodopsin (RHO) was incubated with Fc-tagged DR5 ectodomain domain (long isoform, 500 nM). Signal was obtained by probing with anti-Fc.

B) Coomassie stained SDS-PAGE gel of pulldown on Fc-tagged DR5L ECD (55 kDa) or TNFR1 ECD (65 kDa) incubated with increasing concentrations of the MPZ-ecto^{VD} peptide (apparent MW of 10 kDa, see Table S5 for sequence).

C) Fluorescence quenching of AlexaFluor647-DR5L (green) or TNFR1 ECD (blue) was measured with increasing MPZ-ecto peptide to quantify the binding affinity, whereas quenching was not observed with the mutated MPZ-ecto$^{Tyr\rightarrow Glu}$ peptide (magenta) (N=3, error bars are SD). DR5L ECD binds to the MPZ-ecto peptide with a $K_{1/2}$ of 109 $\pm$ 11 μM with a hill coefficient of 2.6 $\pm$ 0.5.

D) SDS-PAGE of recombinant FLAG-tagged DR5L ECD (25 kDa, 10 μM) incubated with MPZ-ecto peptide at the noted concentrations and treated with the amine crosslinker BS3 (100 μM), probed with anti-FLAG.

E) Size exclusion chromatographs of absorbance at 280 nm for 25 µM recombinant DR5L ECD alone (black), pre-incubated with 100 μM fluorescein-conjugated MPZ-ecto peptide (green) or 100 μM fluorescein-conjugated MPZ-ecto$^{Tyr\rightarrow Glu}$ peptide (magenta).

F) SDS-PAGE gels scanned for fluorescence and then stained with Coomassie for eluted size exclusion fractions in (E). Green outlines (top pair) correspond to fractions from DR5L pre-incubated with MPZ-ecto peptide, and magenta outlines (bottom pair) correspond to DR5L with MPZ-ecto$^{Tyr\rightarrow Glu}$ peptide. Lane marked by "-" denotes a blank lane between the input and 7-ml fraction to minimize spillover of signal from input sample. Arrowheads mark detectable peptide fluorescence in the indicated fractions.

Fig 3–figure supplement 1: DR5 ECD binds to selective subset of sequences displayed by the secretory proteome.

A) Intensity values of each peptide spot in the MPZ section of the peptide array in Fig 3A were normalized to the spot of highest intensity within MPZ. Green box below denotes the peptide chosen as a candidate binder, called MPZ-ecto, shown in spots C18-C19 on the array. Sequences for the peptides are listed in Fig 3–source data 1.

B) Intensity values of the RHO peptide array section in Fig 3A normalized to the highest intensity from MPZ. Peptides were derived from the extracellular N-terminus tail and the extracellular loops (EL1-EL3) that connect the transmembrane domains of rhodopsin.

C) Quantification of enriched amino acids from peptides with an intensity value greater than one standard deviation above the average signal, noted as a preferred peptide, within the entire array. Enrichment ratio for each amino acid was calculated as the frequency of occurrence in preferred peptides divided by its total frequency on the array.

Fig 3–source data 1: Sequences and quantification of peptides probed with Fc-DR5 ECD on the peptide array

This excel file contains the peptide sequences of the peptide array shown in Fig 3A, the quantification of DR5 ECD detected for each spot, and the analysis for enriched amino acids in Fig 3–figure supplement 1.

Fig 3–figure supplement 2: Purified recombinant DR5 ECD oligomerizes with peptide in a specific and reversible manner.

A) Fluorescence scan at 647 nm of SDS-PAGE for gel filtration-purified DR5L (25 kDa) or TNFR1 ECD (35 kDa) labeled with NHS-ester AlexaFluor647. These proteins were used in the fluorescence quenching assays shown in Fig 3C.

B) Fluorescence de-quenching of AlexaFluor647-DR5L ECD (200 nM) pre-incubated with 100 μM or 200 μM of MPZ-ecto peptide in the presence of increasing concentrations of unlabeled DR5L ECD.

C) Coomassie-stained SDS-PAGE of gel filtration purified FLAG-tagged DR5L ECD proteins used for the crosslinking assay in Fig 3D and size exclusion chromatography in Fig 3E.

D) Size exclusion chromatographs of absorbance at 280 nm for recombinant DR5L ECD to show that increased concentration of DR5L alone does not yield multimers.

E) Size exclusion chromatographs of absorbance at 280 nm for recombinant DR5L ECD alone (25 μM, black) or incubated with TRAIL (25 uM, purple). Trace for TRAIL alone (50 μM) is shown in light orange.

F) SDS-PAGE gels stained with Coomassie blue for eluted size exclusion fractions in Fig S8E depicting bands for DR5L ECD and TRAIL.

G) Size exclusion chromatographs of absorbance at 280 nm for 25 μM recombinant DR5L ECD alone (black), pre-incubated with 400 μM fluorescein-conjugated MPZ-ecto peptide (teal).

H) SDS-PAGE gels scanned for fluorescence and then stained with Coomassie for eluted size exclusion fractions in Fig 3–figure supplement 2G. Lane marked by "-" denotes a blank lane between the input and 7-ml fraction to minimize spillover of signal from input sample. Arrowheads mark detectable peptide fluorescence in the indicated fractions.

Fig 4: Disrupting misfolded protein binding to DR5 impairs ER stress-induced apoptosis.

A) Diagram of constructs generated to replace the MPZ ectodomain with the minimal DR5-binding MPZ-ecto peptide (green), the peptide harboring Tyr → Glu mutations (magenta), or the peptide with all aromatic residues (Arom) mutated to Glu (light pink). SS = signal sequence of MPZ, TM = transmembrane domain, ICD = intracellular domain.

B) Western blot of HCT116 cell lysates harvested 24 h post-transfection with 1 μg of MPZ-GFP plasmid, empty vector, or a titration of GFP-tagged MPZ-ecto peptide variants, followed by GFP alone. FL denotes full-length PARP, while C denotes cleaved PARP. The percentage of cleaved PARP was calculated as the signal of cleaved PARP divided by total PARP (FL + C). Arrows denote conditions carried forward for normalized expression levels of the ecto peptide constructs.

C) Fold change in caspase 8 activity relative to GFP expression, as measured by incubation of luminescent caspase glo 8 substrate with lysates from HCT116 transfected using conditions described in Fig 4B lanes 5, 7 and 10 (error bars represent SEM of n = 3 biological replicates; *** denotes $p < 0.005$, and ns indicates $p = 0.18$ from unpaired t-tests with equal SD).

D) RT-PCR for unspliced and spliced forms of *Xbp1* mRNA isolated from HCT116 cells transfected for 24 h with the empty vector +/- 100 nM Tg, or with MPZ-GFP, or MPZ-ecto peptide GFP and its mutant variants (Tyr → Glu and Arom → Glu) using conditions from Fig 4B, lanes 5, 7, and 10.

E) qPCR for reverse-transcribed transcripts harvested from HCT116 cells transfected with the constructs described in 4A, using conditions shown in Fig 4B lanes 5, 7, and 10. (n = 3 biological replicates, * denotes $p < 0.05$ and ns = non-significant).

F) Immunofluorescence for DR5 and ERGIC53 in HCT116 transfected with the MPZ-ecto peptide for 24 hrs. ERGIC53 is magenta in the overlay with MPZ (green) or cyan in the overlay with DR5 (red) (scale bar = 5 μm).

G) Left: Immunoblots of HCT116 lysate inputs expressing the constructs described in 4A, where L and S mark the long and short isoforms of DR5, respectively, and where FL and C mark the full-length and cleaved fragments of PARP, respectively. The percentage of cleaved PARP is quantified as the signal of the cleaved fragment divided by total PARP (FL + C). Right: Immunoprecipitation of GFP-tagged proteins from the lysates shown in (C), where L and S denote the long and short isoforms of DR5, respectively.

H) Average percent of annexin V staining for HCT116 cells transfected as described in C) and D) from n = 3 biological replicates (error bars = SEM, * indicates p = 0.026, and ** indicates p = 0.003 from unpaired t-tests with equal SD). See Fig 4–figure supplement 3 for distribution of early vs late apoptotic cells.

Fig 4–source data 1: Caspase glo 8 measurements for MPZ-ecto peptide expression

This zip archive contains the measured luminescent units for caspase glo 8 activity shown in Figures 4C (lysates) and the coomassie gel used to normalize lysate concentration as a.tif file.

Fig 4–source data 2: qPCR and statistical analysis for expression of MPZ-ecto peptides

This zip archive contains the compiled excel file for qPCR data shown in Fig 4E along with the Prism 6 file used to perform multiple t-tests with Holm-Sidak correction for multiple comparisons.

Fig 4–source data 3: FCS files and quantification of Annexin V staining for MPZ-ecto peptides

This zip archive contains FCS files from n = 3 biological replicates of HCT116 transfected with the conditions outlined in Fig 4H. The excel file contains the quantification of Annexin V staining exported frow FlowJo.

Fig 4–figure supplement 1: Introducing Glu mutations to the DR5-binding sequence of MPZ disrupts PARP cleavage in a DR5-dependent manner.

A) Western blot of HepG2 cell lysates harvested 24 h post-transfection with 1 μg of the empty vector, MPZ-GFP, or a titration of GFP-tagged MPZ-ecto peptide variants. FL denotes full-length PARP, while C denotes cleaved PARP. The percentage of cleaved PARP was calculated as the signal of cleaved PARP divided by total PARP (FL + C).

B) Western blot of HCT116 cell lysates transfected with siRNA against a non-targeting (Nt) sequence or DR5 (referred to as DR5-siRNA-2 in Materials and Methods) for 48 h and co-expressing FLAG-tagged DR5 long isoform and/or MPZ-ecto peptide-GFP.

Fig 4–figure supplement 2: Glu-containing mutants of MPZ-ecto peptide accumulate in the ERGIC.

A) Immunofluorescence for DR5 and ERGIC53 in HCT116 transfected with the MPZ-ecto Tyr-to-Glu peptide for 24 hrs. ERGIC53 is magenta in the overlay with MPZ (green) or cyan in the overlay with DR5 (red) (scale bar = 5 μm).

B) Immunofluorescence for DR5 and ERGIC53 in HCT116 transfected with the MPZ-ecto Arpm-to-Glu peptide for 24 hrs. ERGIC53 is magenta in the overlay with MPZ (green) or cyan in the overlay with DR5 (red) (scale bar = 5 μm).

C) Quantification of Pearson's correlation per cell between ERGIC53 and GFP-tagged peptides of fixed HCT116 cells at 24 h post-transfection with MPZ-ecto peptide (green) and the Glu-containing peptide mutants (dark and light pink). Whisker-box plots depict the Tukey method**.** Statistics were performed through unpaired two-tailed t-tests, where ns indicates $p > 0.50$.

D) Quantification of Pearson's correlation per cell between DR5 and GFP-tagged peptides of fixed HCT116 cells at 24 h post-transfection with MPZ-ecto peptide (green) and the Glu-containing peptide mutants (dark and light pink). Whisker-box plots depict the Tukey method**.** Statistics were performed through unpaired two-tailed t-tests with equal SD, where ns means $p > 0.11$.

E) Table summarizing the mean $\pm$ SEM of the Pearson's correlation per cell shown in Whisker-box plots of C-D.

Fig 4–figure supplement 3: MPZ-ecto peptide engagement of DR5 in cells drives apoptotic cell death.

A) Quantification of the percent of total DR5 recovered in the IPs of GFP-tagged MPZ-ecto peptides, shown in Fig 4G. (n = 2 biological replicates. * denotes p = 0.047, ** denotes p = 0.0054, and ns indicates p = 0.62 from unpaired t-test with equal SD.) The DR5 signal of the input and IP lanes were quantified from the same exposure and then normalized to the amount loaded on the gel. Source data of blots and quantification are provided in Fig 4–source data 4.

B) Flow cytometry measurements of SytoxBlue (405 nm) and annexin V (647 nm) staining of HCT116 transfected with empty vector for 24 h.

C) Flow cytometry measurements of SytoxBlue (405 nm) and annexin V (647 nm) staining of HCT116 transfected with GFP-tagged MPZ-ecto peptide for 24 h.

D) Flow cytometry measurements of SytoxBlue (405 nm) and annexin V (647 nm) staining of HCT116 transfected with GFP-tagged MPZ-ecto peptide and co-treated with 20 μm of z-VAD for 24 h.

E) Flow cytometry measurements of SytoxBlue (405 nm) and annexin V (647 nm) staining of HCT116 transfected with GFP-tagged MPZ-ecto Tyr→Glu peptide for 24 h.

F) Flow cytometry measurements of SytoxBlue (405 nm) and annexin V (647 nm) staining of HCT116 transfected with GFP-tagged MPZ-ecto Arom→Glu peptide for 24 h.

G) Table summarizing percent of cells stained in each quadrant of plots shown in B-F.

Fig 4–source data 4: Westerns and quantification of DR5 recovered on IPs

This zip archive contains .tif files of the Westerns from inputs and IPs of the MPZ-ecto peptides (n = 2 biological replicates) used to quantify the percent of DR5 recovered shown in Fig 4–figure supplement 3A.

Acknowledgements

We thank D. Lawrence at Genentech for gifting anti-DR5 5C7-conjugated agarose beads and helpful discussions. We are grateful to C.M. Gallagher for her detailed immunofluorescence protocols, to G.E. Karagöz for her insight on peptide binding assays, to N.W. Frankel for his help in flow cytometry, to K. Crotty for her quantitative PCR protocol, and to S. Mukherjee for her thoughtful feedback. M. Lam was funded by a National Science Foundation Graduate Research fellowship. S. Marsters is Principal Staff Researcher and A. Ashkenazi is Senior Staff Scientist of Genentech, Inc. P. Walter is an investigator of the Howard Hughes Medical Institute.

Figure 1

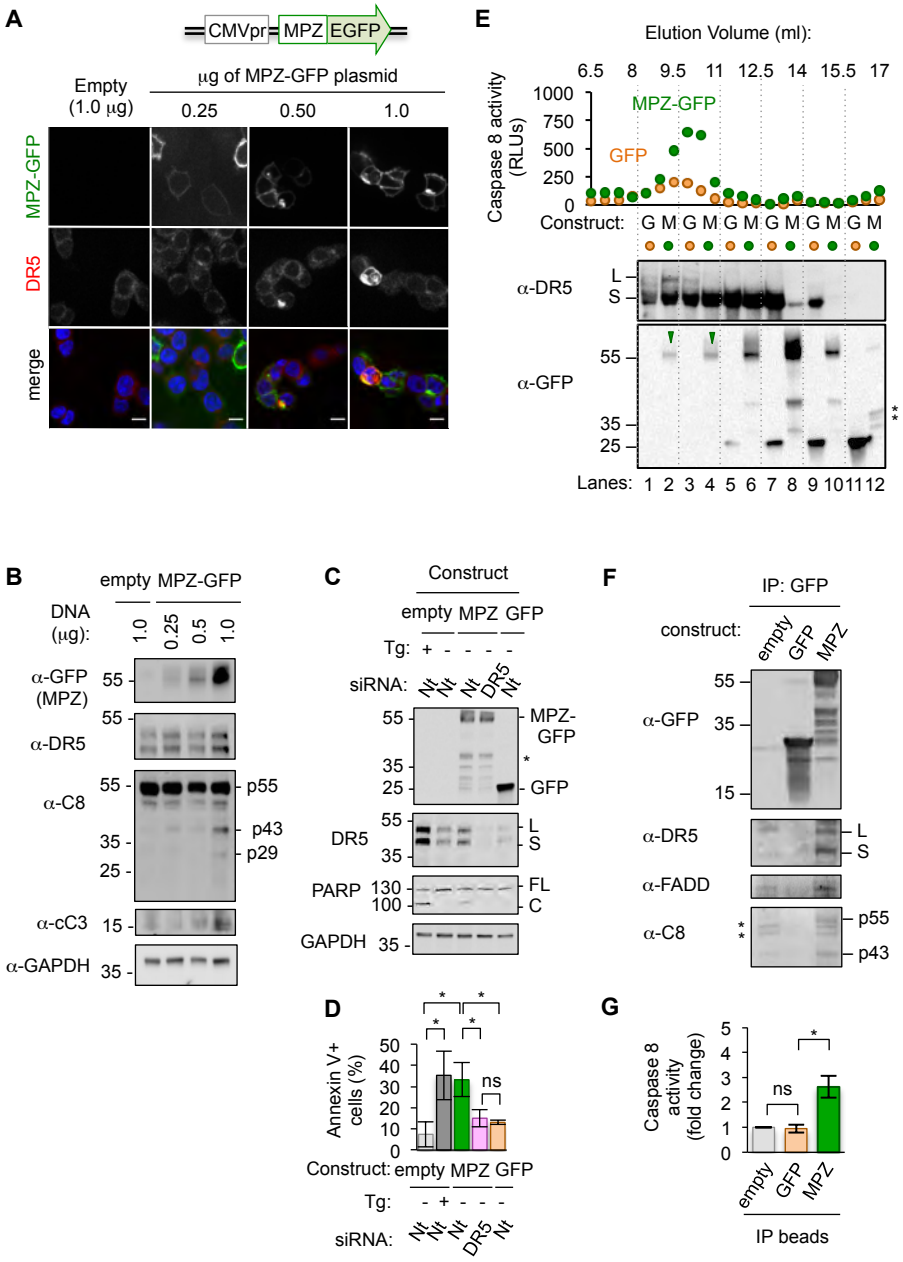
A
CMVpr
MPZ
EGFP
Empty (1.0 μg)
μg of MPZ-GFP plasmid
0.25
0.50
1.0
MPZ-GFP
DR5
merge
E
Elution Volume (ml):
6.5 8 9.5 11 12.5 14 15.5 17
Caspase 8 activity (RLUs)
1000
750
500
250
0
MPZ-GFP
GFP
Construct: G M G M G M G M G M G M
α-DR5
L
S
α-GFP
55
35
25
**
Lanes: 1 2 3 4 5 6 7 8 9 10 11 12
B
empty
MPZ-GFP
DNA (μg):
1.0
0.25
0.5
1.0
α-GFP (MPZ)
55
α-DR5
55
α-C8
55
35
25
p55
p43
p29
α-cC3
15
α-GAPDH
35
C
Construct
empty MPZ GFP
Tg: + - - - -
siRNA: Nt Nt Nt DR5 Nt
55
35
25
MPZ-GFP
*
GFP
DR5
55
35
L
S
PARP
130
100
FL
C
GAPDH
35
D
Annexin V+ cells (%)
50
40
30
20
10
0
*
*
*
*
ns
Construct: empty MPZ GFP
Tg: - + - - -
siRNA: Nt Nt Nt DR5 Nt
F
IP: GFP
construct:
empty
GFP
MPZ
55
35
15
α-GFP
α-DR5
L
S
α-FADD
α-C8
**
p55
p43
G
Caspase 8 activity (fold change)
5
4
3
2
1
0
*
ns
empty
GFP
MPZ
IP beads

Figure 1–figure supplement 1

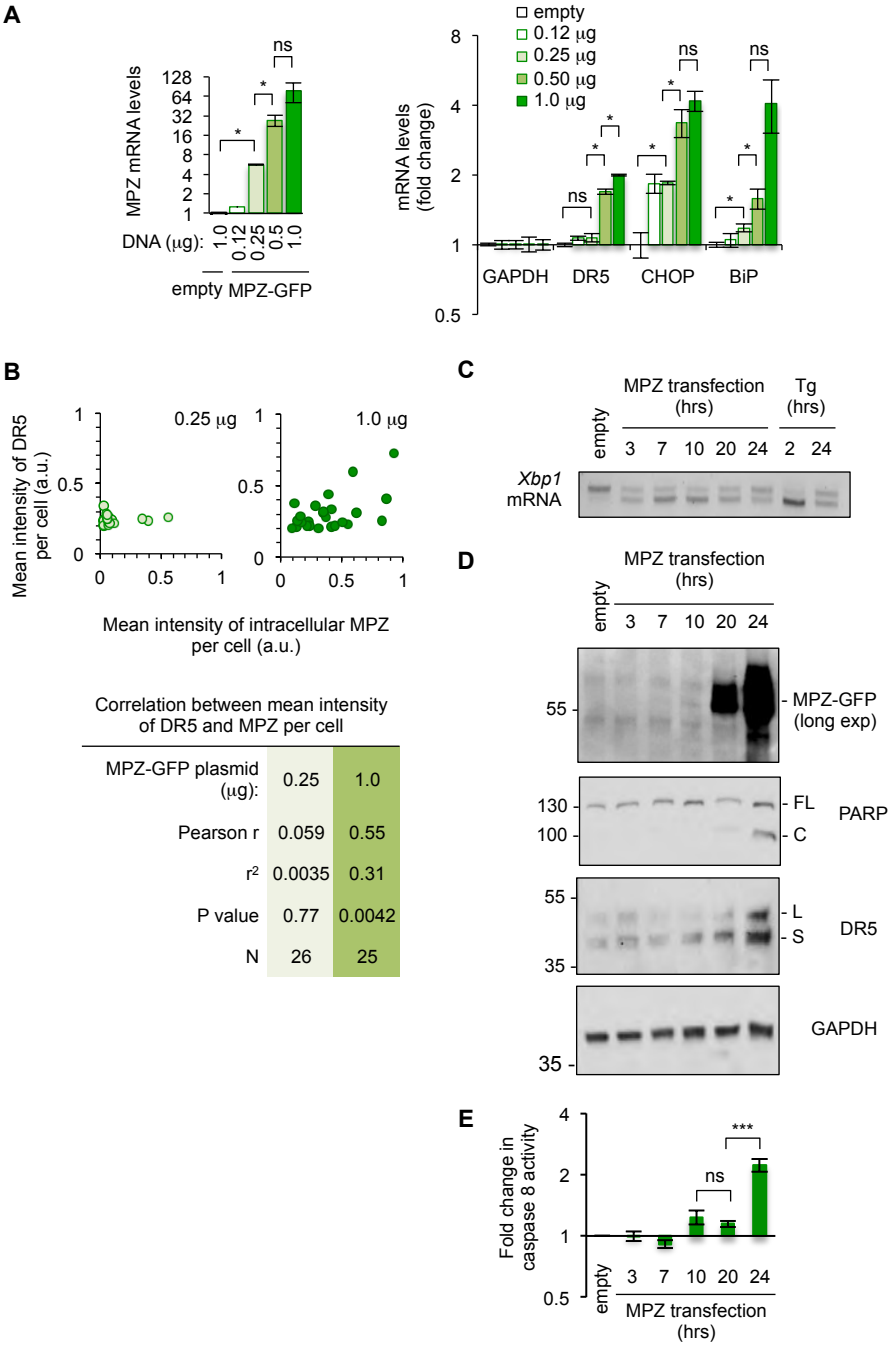

Figure 1–figure supplement 2

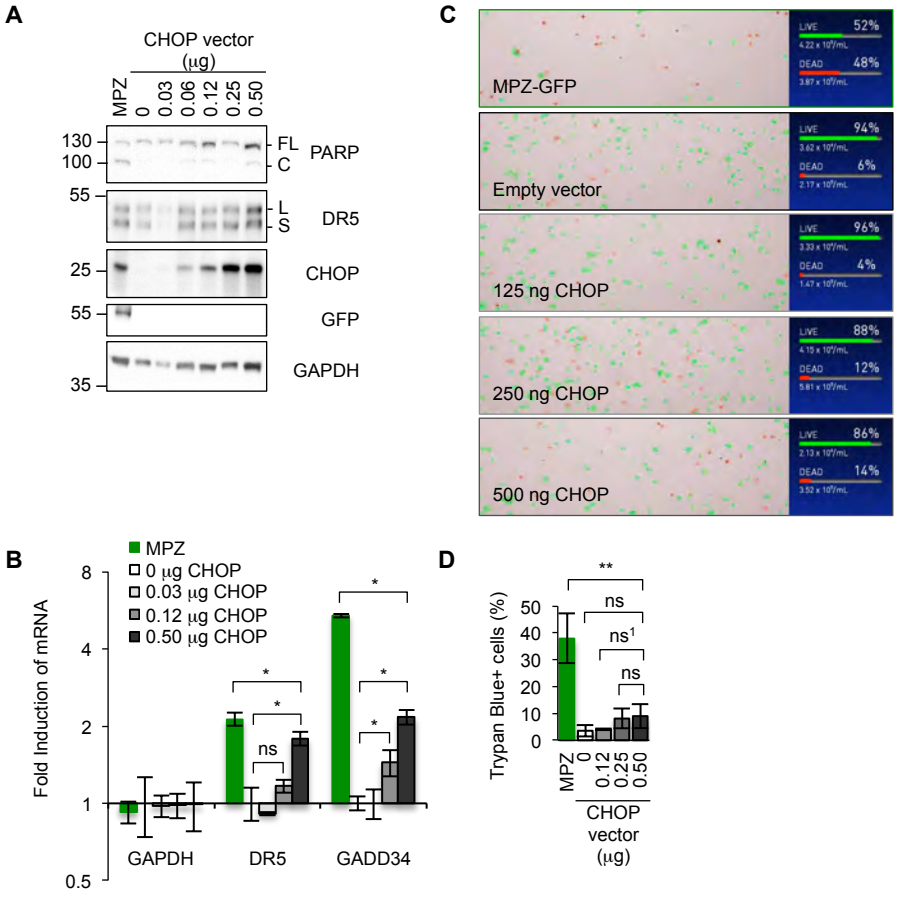

Figure 1–figure supplement 3

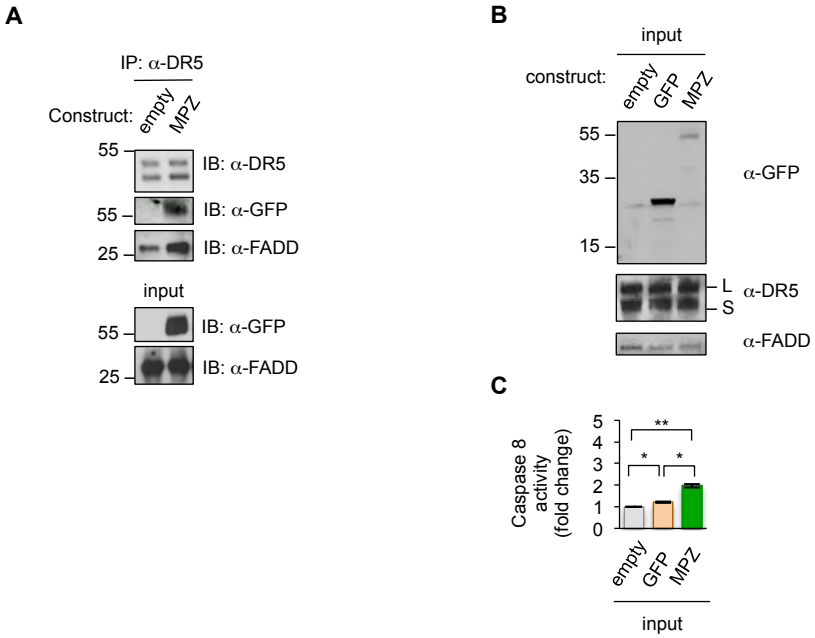

Figure 1–figure supplement 4

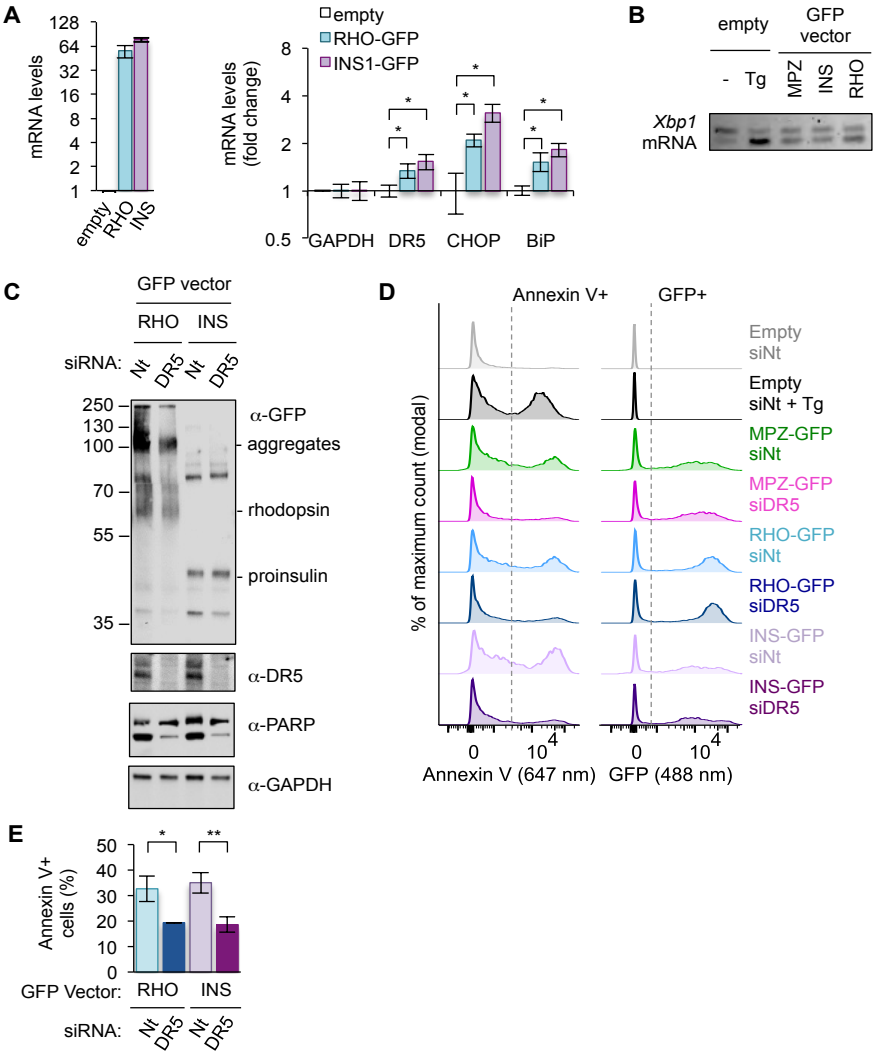

Figure 1–figure supplement 5

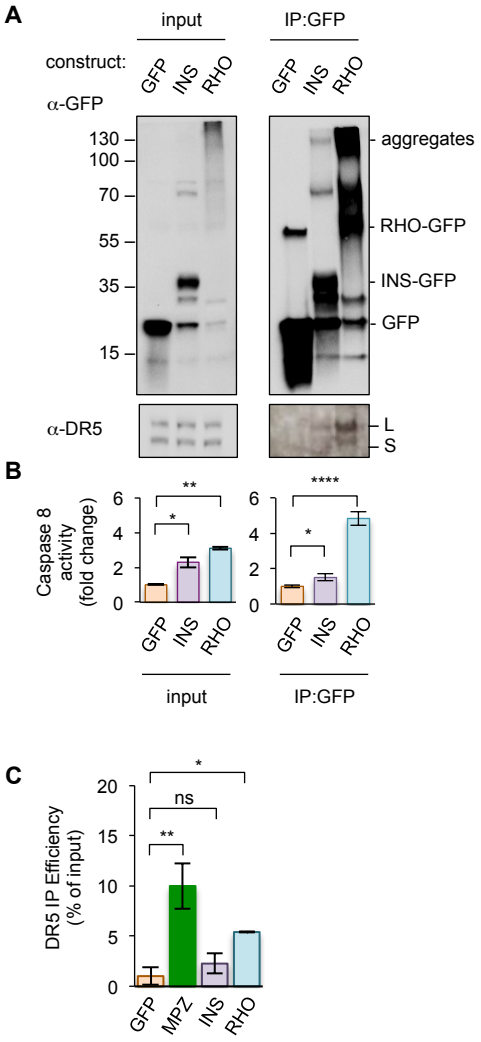

Figure 2

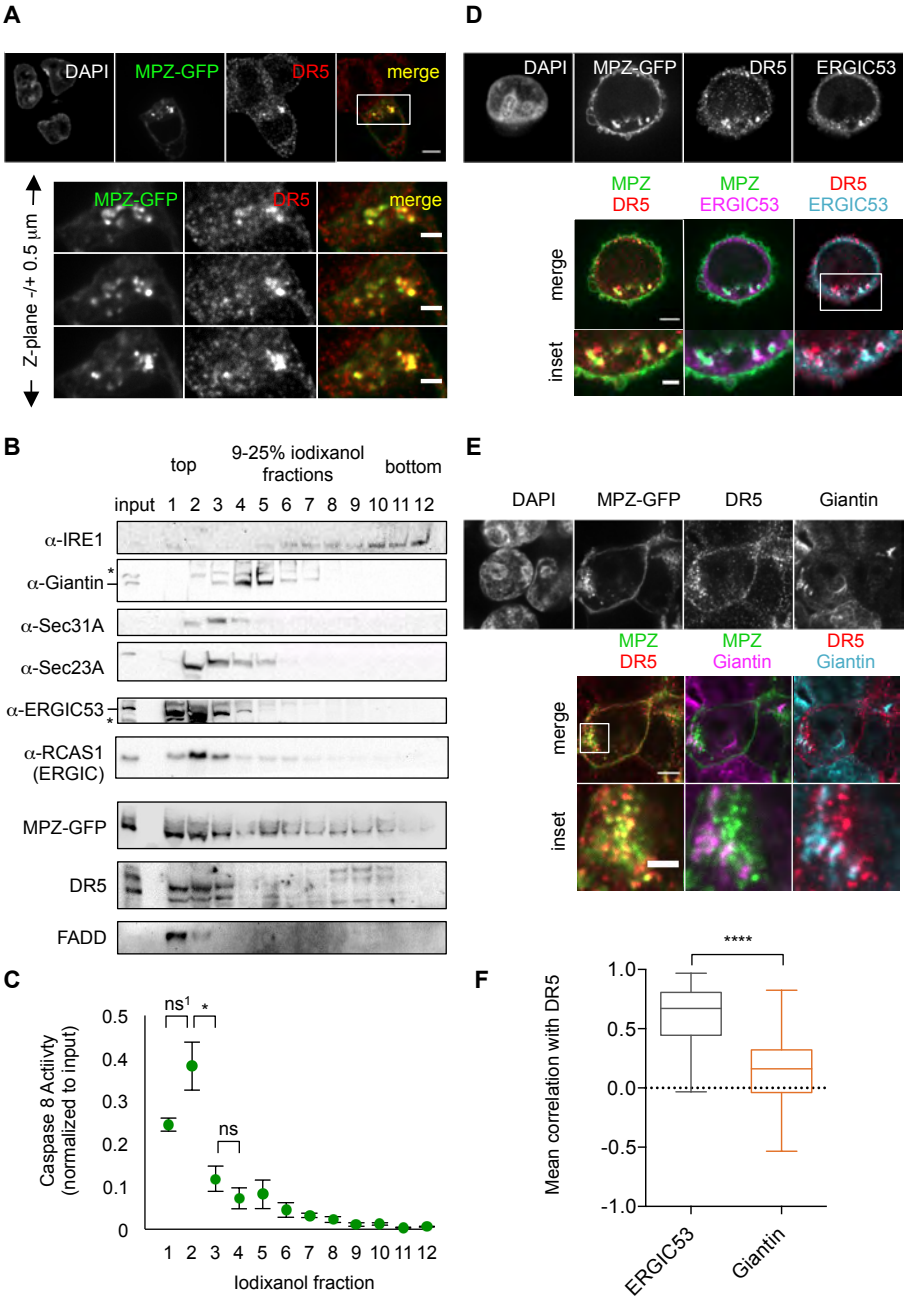
A
DAPI
MPZ-GFP
DR5
merge
Z-plane -/+ 0.5 µm
D
DAPI
MPZ-GFP
DR5
ERGIC53
MPZ DR5
MPZ ERGIC53
DR5 ERGIC53
merge
inset
B
top
9-25% iodixanol fractions
bottom
input 1 2 3 4 5 6 7 8 9 10 11 12
α-IRE1
α-Giantin
α-Sec31A
α-Sec23A
α-ERGIC53
α-RCAS1 (ERGIC)
MPZ-GFP
DR5
FADD
E
DAPI
MPZ-GFP
DR5
Giantin
MPZ DR5
MPZ Giantin
DR5 Giantin
merge
inset
C
Caspase 8 Activity (normalized to input)
ns1
*
ns
Iodixanol fraction
F
Mean correlation with DR5
****
ERGIC53
Giantin

Figure 2–figure supplement 1

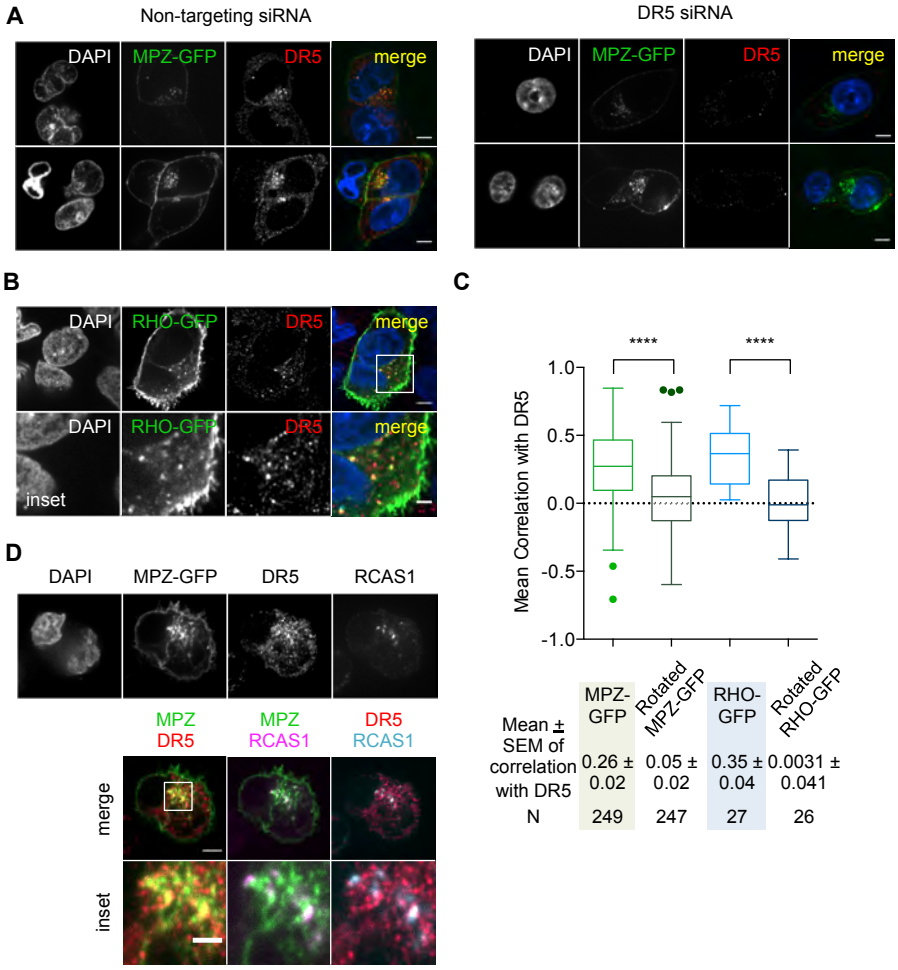

Figure 2–figure supplement 2

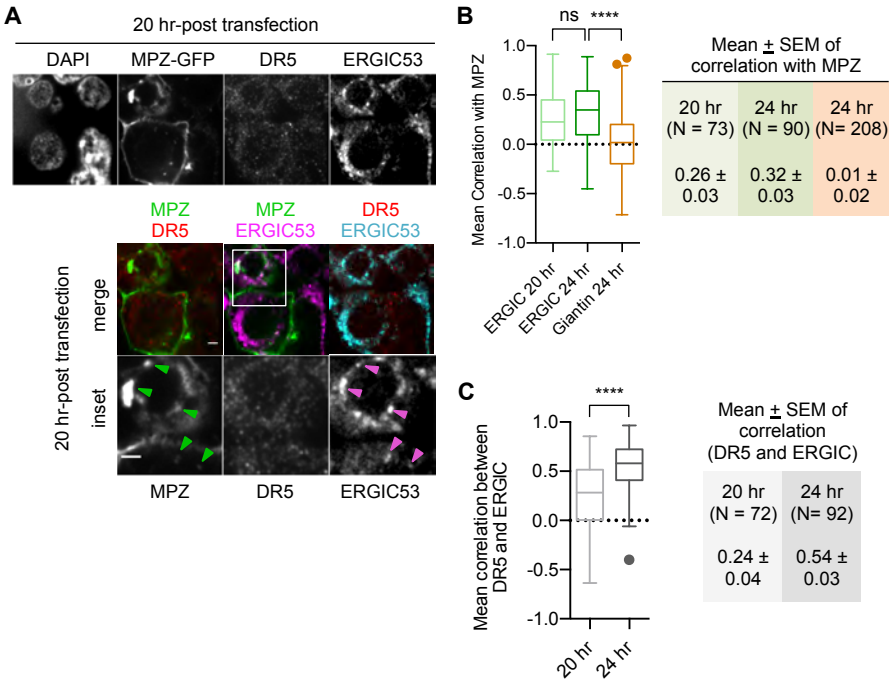

Mean ± SEM of correlation with MPZ		
20 hr (N = 73)	24 hr (N = 90)	24 hr (N= 208)
0.26 ± 0.03	0.32 ± 0.03	0.01 ± 0.02

Mean ± SEM of correlation (DR5 and ERGIC)	
20 hr (N = 72)	24 hr (N= 92)
0.24 ± 0.04	0.54 ± 0.03

Figure 3

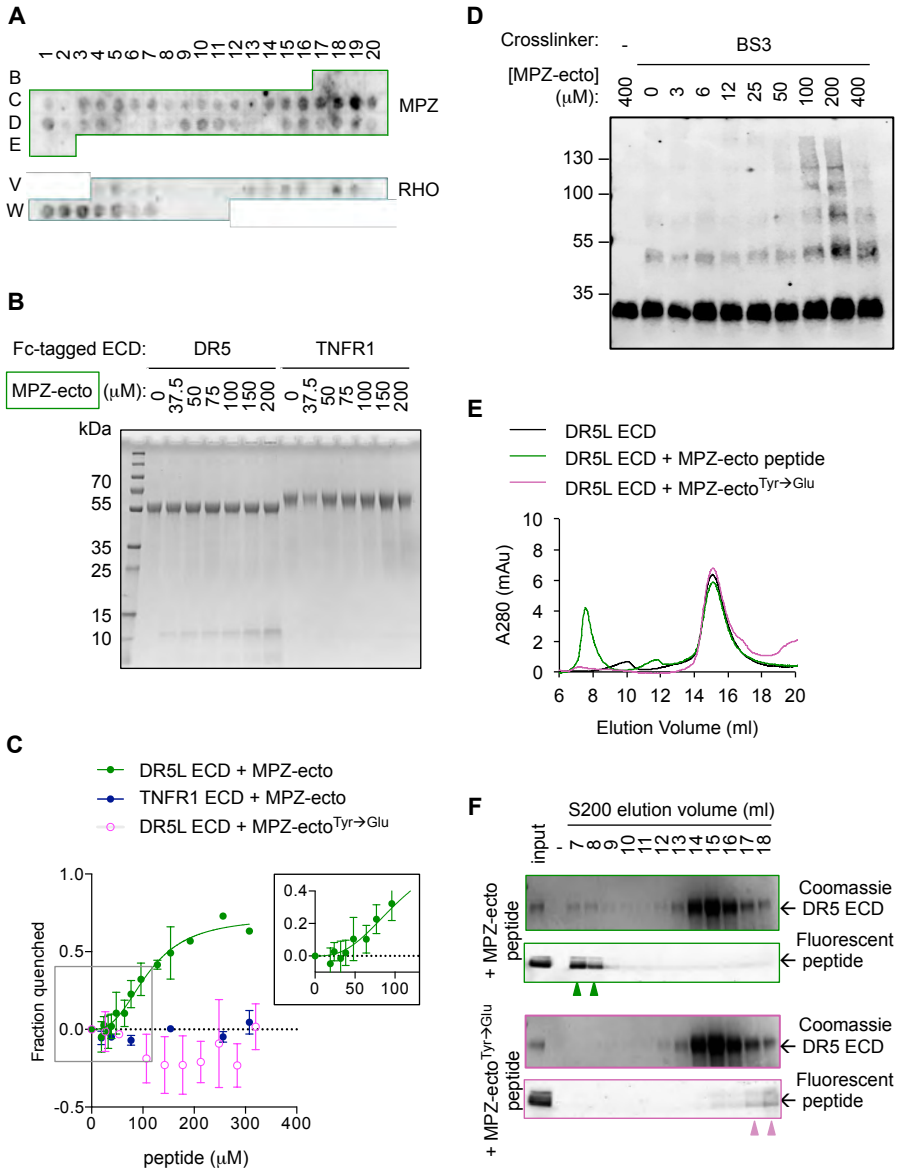
A
1 2 3 4 5 6 7 8 9 10 11 12 13 14 15 16 17 18 19 20
B
C
D
E
MPZ
V
W
RHO
B
Fc-tagged ECD:
DR5
TNFR1
MPZ-ecto (μM):
0 37.5 50 75 100 150 200
0 37.5 50 75 100 150 200
kDa
70
55
35
25
15
10
C
DR5L ECD + MPZ-ecto
TNFR1 ECD + MPZ-ecto
DR5L ECD + MPZ-ecto Tyr→Glu
Fraction quenched
1.0
0.5
0.0
-0.5
0
100
200
300
400
peptide (μM)
0.4
0.2
0.0
0
50
100
D
Crosslinker:
-
BS3
[MPZ-ecto] (μM):
400 0 3 6 12 25 50 100 200 400
130
100
55
35
E
DR5L ECD
DR5L ECD + MPZ-ecto peptide
DR5L ECD + MPZ-ecto Tyr→Glu
A280 (mAu)
10
8
6
4
2
0
6 8 10 12 14 16 18 20
Elution Volume (ml)
F
S200 elution volume (ml)
input
- 7 8 9 10 11 12 13 14 15 16 17 18
+ MPZ-ecto peptide
Coomassie
DR5 ECD
Fluorescent
peptide
+ MPZ-ecto Tyr→Glu peptide
Coomassie
DR5 ECD
Fluorescent
peptide

Figure 3–figure supplement 1

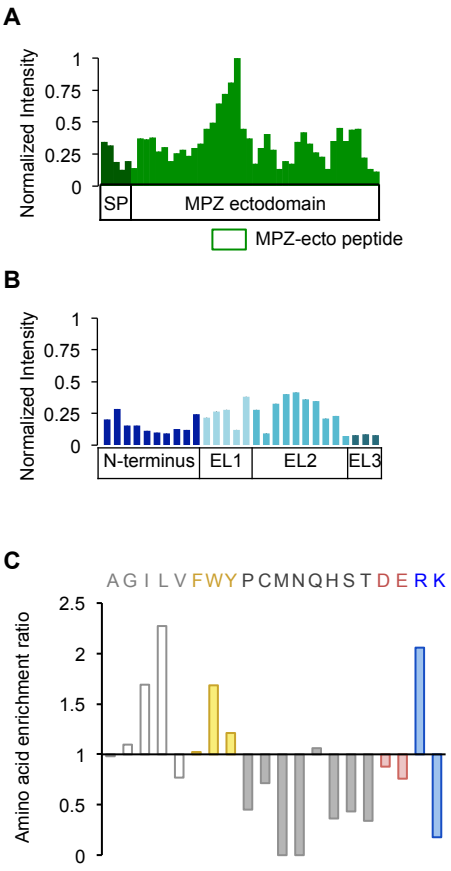

Figure 3–figure supplement 2

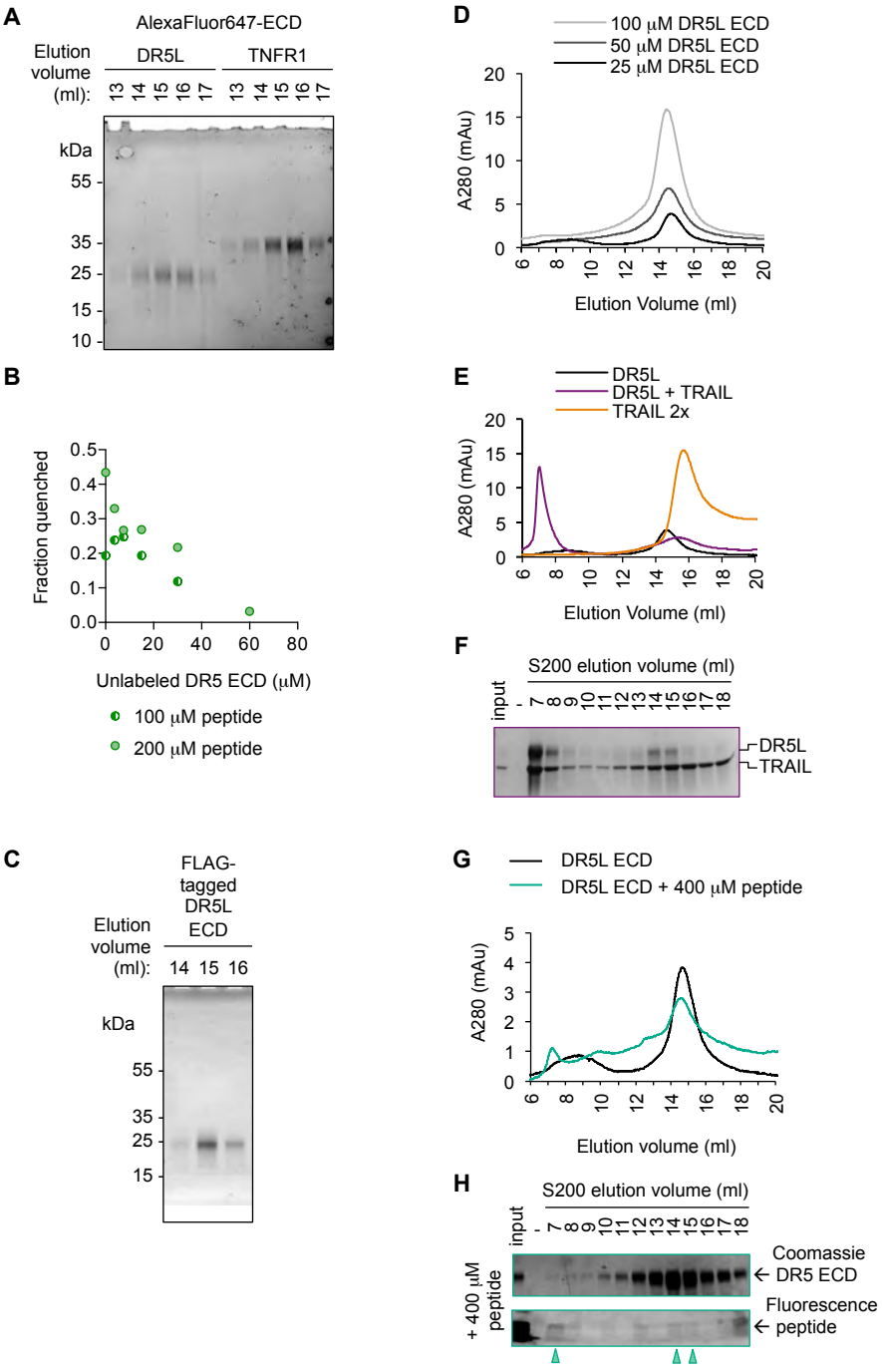

Figure 4

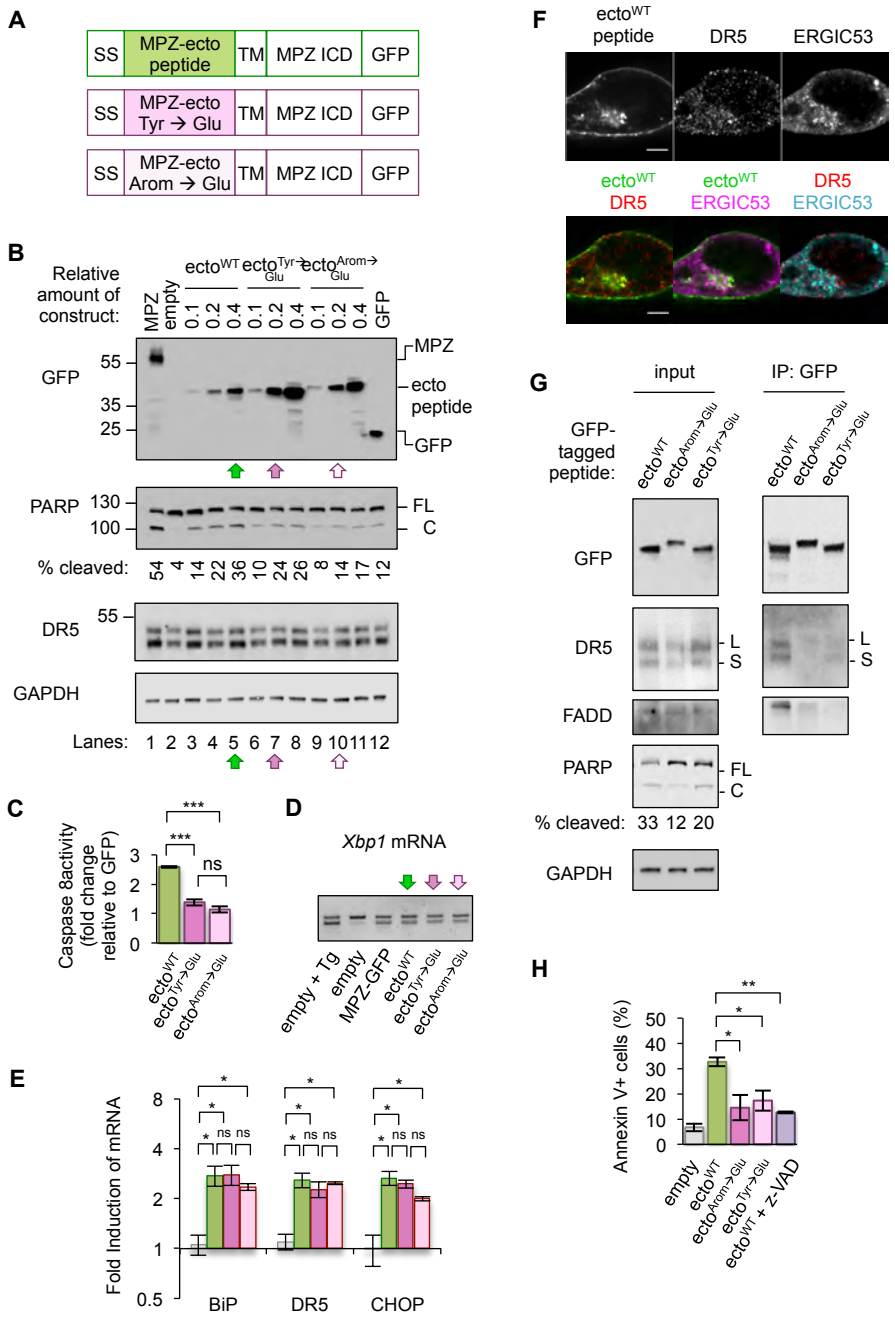
A
SS
MPZ-ecto peptide
TM
MPZ ICD
GFP
SS
MPZ-ecto Tyr → Glu
TM
MPZ ICD
GFP
SS
MPZ-ecto Arom → Glu
TM
MPZ ICD
GFP
B
Relative amount of construct:
ectoWT
ectoTyr→Glu
ectoArom→Glu
MPZ
empty
0.1
0.2
0.4
0.1
0.2
0.4
0.1
0.2
0.4
GFP
GFP
55
35
25
MPZ
ecto peptide
GFP
PARP
130
100
FL
C
% cleaved:
54 4 14 22 36 10 24 26 8 14 17 12
DR5
55
GAPDH
Lanes: 1 2 3 4 5 6 7 8 9 10 11 12
C
Caspase 8activity (fold change relative to GFP)
***
***
ns
3
2
1
0
ectoWT
ectoTyr→Glu
ectoArom→Glu
D
Xbp1 mRNA
empty + Tg
empty
MPZ-GFP
ectoWT
ectoTyr→Glu
ectoArom→Glu
E
Fold Induction of mRNA
8
4
2
1
0.5
*
*
ns ns
BiP
DR5
CHOP
F
ectoWT peptide
DR5
ERGIC53
ectoWT DR5
ectoWT ERGIC53
DR5 ERGIC53
G
input
IP: GFP
GFP-tagged peptide:
ectoWT
ectoArom→Glu
ectoTyr→Glu
GFP
DR5
L
S
FADD
PARP
FL
C
% cleaved: 33 12 20
GAPDH
H
Annexin V+ cells (%)
50
40
30
20
10
0
**
*
*
empty
ectoWT
ectoArom→Glu
ectoTyr→Glu
ectoWT + z-VAD

Figure 4–figure supplement 1

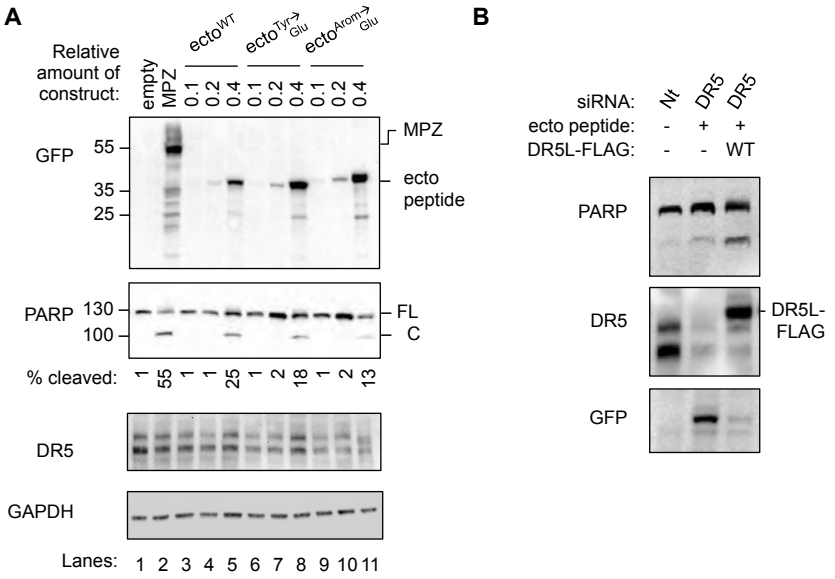

Figure 4–figure supplement 2

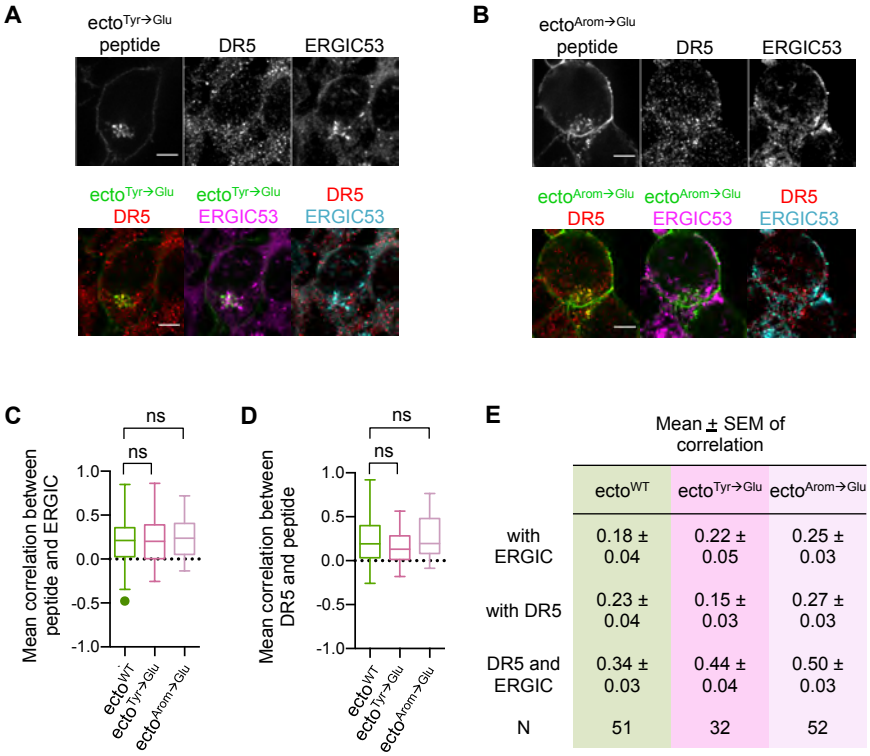

E

	Mean ± SEM of correlation		
	ectoWT	ectoTyr→Glu	ectoArom→Glu
with ERGIC	0.18 ± 0.04	0.22 ± 0.05	0.25 ± 0.03
with DR5	0.23 ± 0.04	0.15 ± 0.03	0.27 ± 0.03
DR5 and ERGIC	0.34 ± 0.03	0.44 ± 0.04	0.50 ± 0.03
N	51	32	52

Figure 4–figure supplement 3

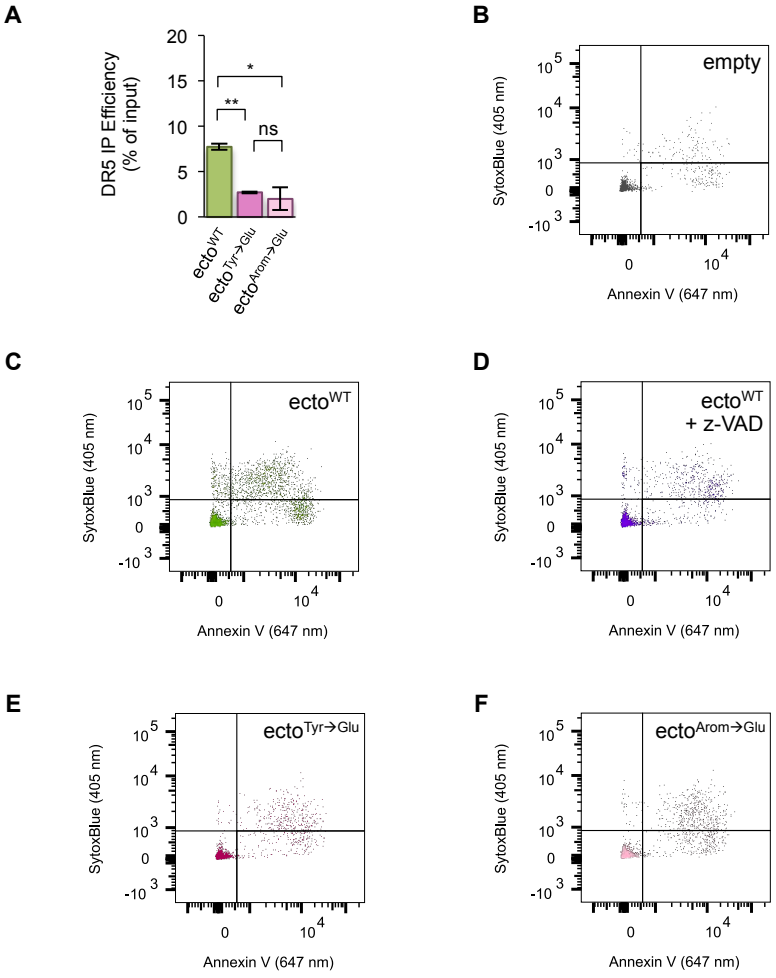

G

Annexin V	Sytox Blue	empty vector	ecto^{WT}	ecto$^{Tyr→Glu}$	ecto$^{Arom→Glu}$	ecto^{WT} + z-VAD
-	-	94.7	65.3	90.3	86.5	86.3
+	-	2.68	11.5	3.64	4.89	3.77
+	+	2.39	19.1	5.66	8.17	8.37
Total # of cells		25595	31661	26969	22594	26634